



#### **BASIC SCIENCE**

Nanomedicine: Nanotechnology, Biology, and Medicine 42 (2022) 102542



## Original Article

nanomedjournal.com

## Glyco-nanotechnology: A biomedical perspective

Mausam Kalita, PhD<sup>a,\*</sup>, Macy M. Payne<sup>b</sup>, Stefan H. Bossmann, PhD<sup>c,\*</sup>

<sup>a</sup>Department of Radiology and Biomedical Imaging, University of California, San Francisco, CA, USA <sup>b</sup>Department of Chemistry, Kansas State University, Manhattan, KS, USA

<sup>c</sup>The University of Kansas Cancer Center–Drug Discovery, Delivery and Experimental Therapeutics, The University of Kansas Medical Center-Cancer Biology, Kansas City, KS

Revised 8 February 2022

#### **Abstract**

Glycans govern cellular signaling through glycan-protein and glycan-glycan crosstalk. Disruption in the crosstalk initiates 'rogue' signaling and pathology. Nanomaterials supply platforms for multivalent displays of glycans, mediate 'rogue' signal correction, and provide disease treatment modalities (therapeutics). The decorated glycans also target overexpressed lectins on unhealthy cells and direct metal nanoparticles such as gold, iron oxide, and quantum dots to the site of infection. The nanoparticles inform us about the state of the disease (diagnosis) through their distinct optical, magnetic, and electronic properties. Glyco-nanoparticles can sense disease biomarkers, report changes in protein-glycan interactions, and safeguard quality control (analysis). Here we review the current state of glyco-nanotechnology focusing on diagnosis, therapeutics, and analysis of human diseases. We highlight how glyco-nanotechnology could aid in improving diagnostic methods for the detection of disease biomarkers with magnetic resonance imaging (MRI) and fluorescence imaging (FLI), enhance therapeutics such as anti-adhesive treatment of cancer and vaccines against pneumonia, and advance analysis such as the rapid detection of pharmaceutical heparin contaminant and recombinant SARS-COV-2 spike protein. We illustrate these progressions and outline future potentials of glyco-nanotechnology in advancing human health.

© 2022 The Author(s). Published by Elsevier Inc. This is an open access article under the CC BY-NC-ND license (http://creativecommons.org/licenses/by-nc-nd/4.0/).

Key words: Glyconanotechnology; Carbohydrates; Analytical; Biomarkers; Diagnostics; Glyco-magnetics; Therapeutics; Infectious disease; Cancer

Nanotechnology has revolutionized biomedical sciences and our fight against human diseases, delivering major weapons with diagnostic, therapeutic, and analytic applications. The metal nanomaterials (gold, iron oxide, and quantum dots), with a diameter one-thousandth the width of a strand of hair, display distinct optical, magnetic, and electronic properties. They inform us about the state of the diseases, participate in the therapeutic intervention, and assay disease markers. Heavy investment in the research and development of nanotechnology has yielded Food and Drug Administration (FDA)-approved thermal therapy, imaging agents, therapeutic monitoring, and iron supplements for chronic kidney disease.

Glyco-nanotechnology combines the surprising nano-range properties with glycoscience. Glycans decorate nearly all cell membrane proteins and occasional lipids in the extracellular matrix (ECM). They mediate not only intra- and inter-cellular communication, but also cell-microbe interactions through a triad of ligand recognition, binding, and cellular signaling.<sup>6,7</sup>

Disruption of the triad breaks the flow of information, resulting in various pathologies such as cancer, neurodegenerative diseases, and microbial infections. Dysregulation of glycan abundance on the cell surface, altered structure and conformation of glycans/glycan-binding proteins, and expression of certain cell surface antigens can contribute to the disruption of the triad.  $^{8-10}$ 

The glyco-nanoparticles (GNPs) target aberrant ECM of diseased tissue, report their changes in the form of optical, magnetic, and electric effects, and detect pathology. <sup>11–13</sup> For example, sialyl Lewis <sup>X</sup>-iron oxide detects brain injury associated lectins through MRI, <sup>14</sup> gold-hyaluronic acid-dye senses metastatic cancer, <sup>15</sup> and quantum dot-hyaluronic acid identifies liver cirrhosis induced CD44 receptor expressions through fluorescence imaging. <sup>16</sup> Additionally, GNPs have been engineered to correct aberrant cellular signaling in diseased cells as nanoparticles display multiple glycan ligands to the proteins or other glycans of cells, initiate molecular interactions, and likely signal

E-mail address: sbossmann@kumc.edu (S.H. Bossmann).

https://doi.org/10.1016/j.nano.2022.102542

1549-9634/© 2022 The Author(s). Published by Elsevier Inc. This is an open access article under the CC BY-NC-ND license (http://creativecommons.org/licenses/by-nc-nd/4.0/).

<sup>\*</sup> Corresponding authors.

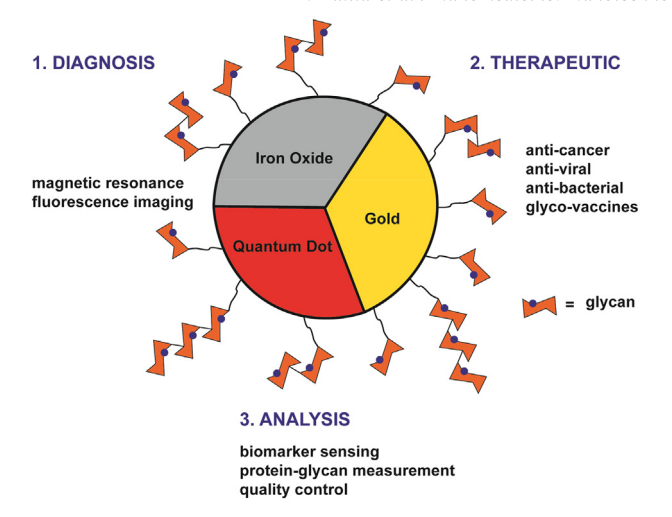


Figure 1. Three main applications of glyco-nanotechnology: (1) diagnosis, (2) therapeutic, and (3) analysis.

transduction. Gold-cluster lactose nanomedicine competes with endothelial cell's glycosphinglipids, detaches them from cancer's stranglehold, and reduces cancer progression. To GNPs also elicit an immune response against tumor-associated carbohydrate antigens (TACAs), making them glyco-vaccines. Gold-mannose imitates human immunodeficiency virus-1 (HIV-1) glycoprotein 120 (gp120), disrupts gp120/dendritic cell receptor interface, and presents anti-HIV treatment potential. The physical and chemical properties of GNPs are modulated to construct potent analytical tools: gold-mannose senses liver cancer biomarkers in serum, electrochemical detection of breast cancer associated O-linked glycans, measure glycan-protein binding constants, and gold-heparin-dye protects the integrity of pharmaceutical grade heparin.

In this review, we examine the diagnostic, therapeutic, and analytical roles of GNPs, focusing on cancer, infectious diseases, and neurological problems. Finally, we will discuss the future potentials of emerging glyco-nanotechnology (Figure 1).

#### Analytical

#### Biomarker sensing

He, X.-P. et al developed gold-mannose glyco-nanoprobes for rapid serological detection on a microplate reader of α-fetoprotein-L3 (AFP-L3), a hepatocellular carcinoma biomarker. <sup>20</sup> The authors leveraged the affinity between  $\alpha$  1-6 fucose residue of AFP-L3 and *Lens culinaris* lectin (LCA), <sup>24</sup> a mannose binding legume lectin. In an AFP-L3 sensing assay the gold-mannose probe competed with the α 1-6 fucose residue of AFP-L3 to occupy the binding sites of LCA. The assay involves two steps. The initial self-aggregation of gold-mannose, mediated by LCA, where a gradual bathochromic shift accompanied by peak broadening of the gold-mannose suggests supramolecular selfaggregation. Following the initial aggregation step is a 10 min incubation of surface-immobilized AFP-L3 biomarker with goldmannose@LCA aggregate. The competitive interaction disaggregates the gold-mannose from LCA, releases gold-mannose into the solution, and reestablishes AFP-L3@LCA interaction.

In a 96-well microplate coated with anti-AFP-L3 antibody, various concentrations of AFP-L3 were first immobilized. Next. gold-mannose@LCA solution was incubated for 10 min while shaking. A microplate reader reported the optical density at  $\lambda =$ 525 nm for each well (Figure 2), a calibration curve was constructed by plotting gold-mannose absorbance (Y-axis) versus concentration of AFP-L3 (X-axis), and this plot was used to calculate the AFP-L3 biomarker concentrations in the test samples. The biantennary N-glycan- $\alpha$ - sialoside labeled quantum dot (QD-A2PC) was used to screen and discover novel hemagglutinin (HA) inhibitors for use in anti-influenza drugs.<sup>25</sup> The assay involved BroHA residue, which binds sialic acid derivatives, of X-31 viral strain. The sialic acid ligands on the glyco-nanoprobe and synthetic compounds compete with each other for BroHA. Competitive fluorescence polarization (FP) determined the inhibitors binding against A2-PC-QD@BroHA by using the following equation  $^{26,27}$ :

$$P = (I_{\text{parallel}} - I_{\text{perpendicular}}) / (I_{\text{parallel}} + I_{\text{perpendicular}})$$

 $I_{\rm parallel}$  is the fluorescence component parallel to the linearly polarized light used for excitation and  $I_{\rm perpendicular}$  is the fluorescence component perpendicular to excitation. The QD-A2PC was excited with vertical polarized light ( $\lambda_{\rm ex}$  = 485 nm) and the intensity of the emitted light was observed through vertical and horizontal polarizers ( $\lambda_{\rm em}$  = 546 nm). A large FP value for QD-A2PC and BroHA interaction suggests slow rotation of the large molecules in the excited state. A dose-dependent inhibitory effect on this FP value can evaluate the inhibitory potency of small molecules. The study resulted in identifying a few potential inhibitors (Figure 3).

An electrochemical assay involving cadmium cations (Cd<sup>2+</sup>) detected the mannose composition of a mammalian cell surface through competitive binding. 28 The cell surface glycan competed with its mimic, a self-assembled poly-mannose, to bind CdTe QD-concanavalin A (mannose binding lectin) nanoprobe. The assay started with a self-assembled monolayer (SAM) of poly-mannose on a gold surface. Next, human leukemia K562 cell surface mannose sugar competed with surface-confined poly-mannose to bind QD-concanavalin A. Atomic force microscopy (AFM) determined the particle size after interaction. An increase in size demonstrated effective recognition of QDconcanavalin A to poly-mannose SAM, while OD-non-mannose binding lectin@ poly-mannose SAM remained unchanged in size. Finally, nitric acid dissolved CdTe ODs on the mannan SAM to produce a solution containing Cd<sup>2+</sup> cations for anodic stripping voltammetric detection of the cell surface mannose (Figure 4). The calibration curve established a linear relationship between the stripping peak current and the logarithm of cell concentration. The Cd<sup>2+</sup> concentration on mannan SAM decreased as more K562 cells were added to the media. This study estimated 6.9 pg or  $2.3 \times 10^{10}$  mannose sugar on each K562 cell.

The cholera toxin, an AB<sub>5</sub> hexameric protein (CTB), binds the pentasaccharide residue of the GM1 ganglioside receptors (glycolipid) in the small intestine. Schofield et al synthesized gold-lactose nanoparticles (Au-lactose) that mimic the

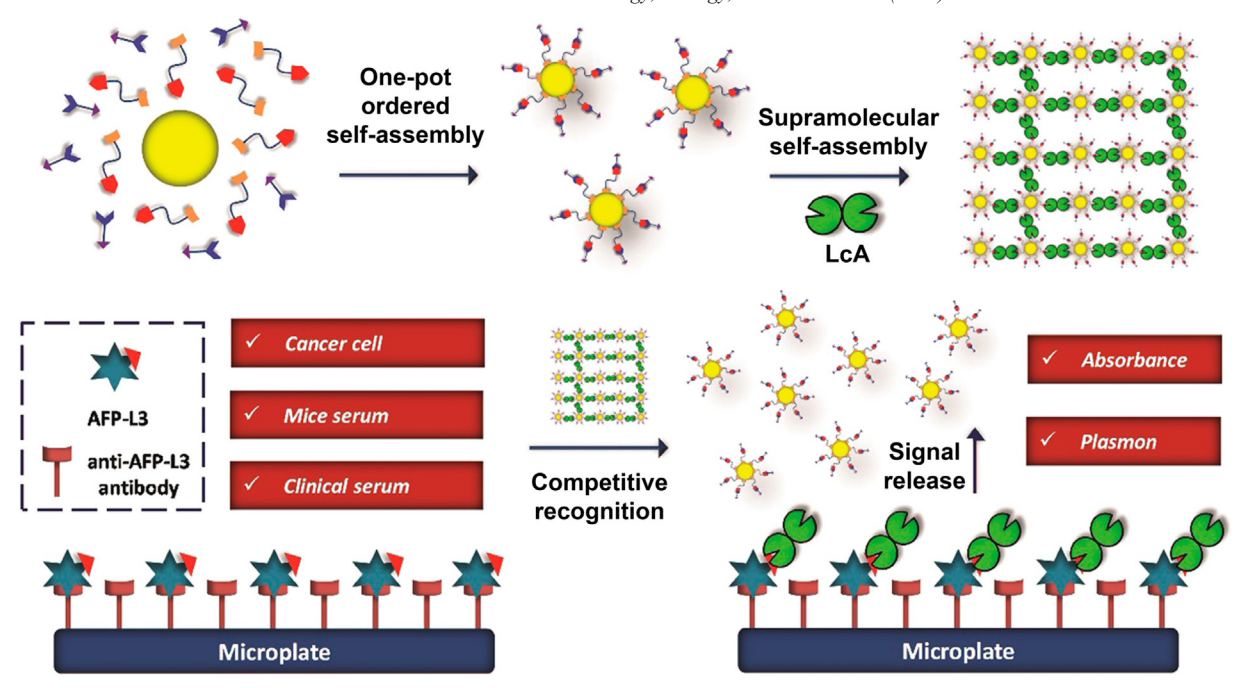


Figure 2. "Self-assembly of the glyco-AuNP followed by formation of the supramolecular glycoprobe via glycoligand–receptor recognitions and use of the resulting glycoprobe to detect  $\alpha$ - fetoprotein-L3 (AFP-L3) immobilized on a microplate from various biological samples" with permission from He X-P, Hu X-L, Jin H-Y, et al. *Anal. Chem.* 87(17), 9078–9083 (2015), copyright American Chemical Society, Washington, DC, 2015.

pentasaccharide residue of GM1 receptors and developed a rapid colorimetric bioassay for CTB.<sup>29</sup> The CTB mediated Aulactose aggregation, broadened the surface plasmon absorption band at  $\lambda = 524$  nm, and shifted the color of solution from red to deep purple. Increase in toxin concentration increased the intensity of the absorbance by forming larger aggregates, with maximum change in absorbance ( $\Delta$ ) at  $\lambda = 620$  nm. The method can detect 110 nM (6.2 µg/mL) CTB within 10 min (Figure 5).

#### Measuring protein-glycan interactions

Jeong et al applied QD-lectin nanoprobes and cell patterning technology to develop a surface glycan profiling method of live cells (cancerous versus normal cells). A library of quantum dot (QD)-lectin probes was developed to map glycan epitopes of cell and tissue surfaces by exploiting lectin–glycan interactions (Table 1). For example, the wheat germ agglutinin (WGA) lectin binds the terminal *N*-acetyl-glucosamine (GlcNAc) and sialic acid epitopes. However, Lotus-tetragonolobus (LTL) binds fucose, Sialyl Lewisx (SLeX), and Lewisx (LeX)) of a cell.

Soft lithography patterned cells in a culture plate were incubated with various lectin-biotin nanoconjugates for 3 h at 37 °C. After washing off non-specific binding, the QD-streptavidin was added for 1 h at 37 °C. The QD-streptavidin recruited the lectin-bound cell surface glycans. The fluorescence microscope identified these glycan epitopes. The QD-WGA identified significantly higher numbers of terminal GlcNAc and sialic acid residues in MCF-7 breast cancer cells compared to human dermal fibroblast (HDF) cells. The library of lectins also informed the nature of glycosidic bonds. MCF-7 cells expressed the GalNAc/Gal and GlcNAc/sialic acid  $\alpha$ -2,6 linkage, while HCT116 colon cancer cells display GlcNAc/sialic acid  $\alpha$ -2,3

linkages.<sup>34</sup> This approach enabled glycan heatmaps for live cancerous and normal cell and tissue samples.

Breast cancer cells overexpress truncated O-linked glycans (β-D-Gal-[1,3]-D-GalNAc disaccharide or T antigens) on the MUC1 protein. An electrochemical assay for Cd2+ ions (supplied by CdS-glycans) can detect the T antigens leveraging lectin-glycan interactions. 21 The assay follows three steps: a) formation of a lectin (peanut agglutinin, PNA) monolayer on a gold surface, b) competition between CdS-glycans and breast cancer T antigens for lectins, and c) determination of cell surface glycans through electrochemical stripping detection of the captured CdS by dissolving lectin bound CdS-glycans in nitric acid (0.1 M, 100 µL). More abundant cell surface glycans produced sharper declines in the Cd2+ stripping peak i.e. more current. The assay showed a sensitivity trend based on the rate of decrease in current (micro Ampere): β-D-Gal-[1,3]-D-GalNAc (65%) > Gal (45%) > GalNAc (20%) at 11.1  $\mu$ M for each glycan. Thus, the breast cancer expresses abundant β-D-Gal-[1,3]-D-GalNAc. This assay might identify defective glycan biomarkers in various disease models.

Cyanovirin-N (CV-N), an 11 kDa cyanobacterial lectin, exhibits HIV gp120 inhibition at nanomolar concentrations. Inspired by the rich Manα1-2Manα scaffolds present on CV-N, two low-mannoses (LM) are conjugated with Au NPs resulting LM-GNPs.<sup>35</sup> The conjugation takes advantage of a photocoupling reaction between perfluorophenylazide (PFPA)-disulfide and LM generating *manno*-GNPs (GNP-M2 and GNP-M3). (Figure 6) These LM-GNPs were used to study their binding for two variants of CV-N, CVN Q50C, and CVN MutDB. CVN Q50C represents a wild-type variant with glycan binding sites A and B, with a cysteine mutation at position 50 for targeted fluorophore labeling, while CVN MutDB is the mutant version

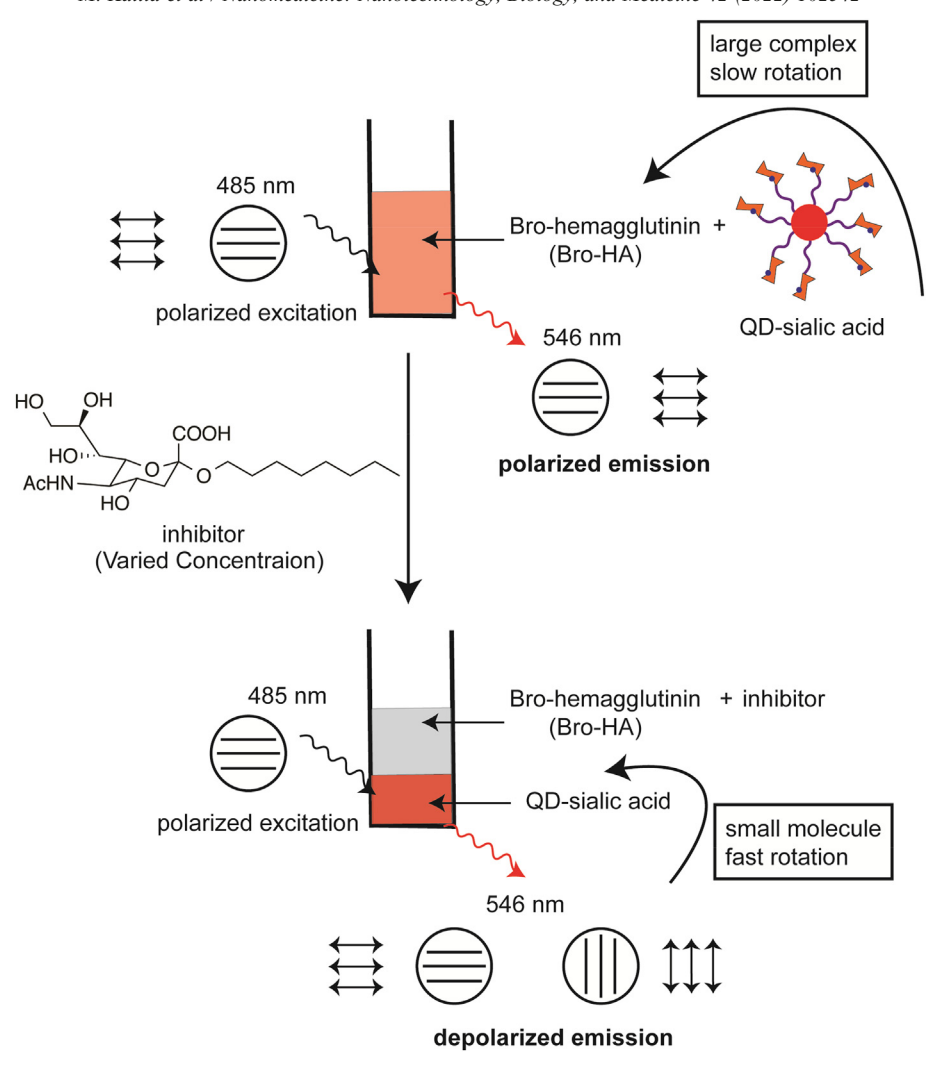


Figure 3. Fluorescence polarization-based assay to screen hemagglutinin blockers. Slow rotation of large QD-sialic acid (or QD-A2PC)@Bro-HA complex resulted in polarized emission with high polarization value. Addition of inihitior competed with QD-sialic acid for Bro-HA, formed inhibitor@Bro-HA complex, and freed the QD-sialic acid. The QD-sialic acid rotated faster leading to depolarized emission with low polarization value. This weighted average of the high and low polarization values gives fluorescence polarization (P).

without domain B, the gp120 binding site. The SPR binding assay showed that LM-GNPs required a gp120-binding site in CV-N for strong interaction. Fluorescence competition binding assay determined the binding affinities, K<sub>D1</sub> (Domain A) and  $\rm K_{D2}$  (Domain B), between GNP-M2 (or GNP-M3) and CVN  $^{\rm Q50C}$  . In this study, Cy5 dye labeled CVN  $^{\rm Q50C}$  (1.2  $\rm \mu M$ , 0.1 mL) was added to free M2 or M3 (0.48 mM, 0.1 mL) to produce a series of GNP-M2 or GNP-M3 solutions (between 5 nM and  $1 \times 10^{-8}$  nM, 1 mL). The solutions were shaken (1 h), centrifuged (30 min), and separated from nanoparticle pellets. The fluoresence intensities of the supernatants were then measured (excitation = 649 nm, emission = 666 nm). The difference in fluorescence intensity of Cy5-CVN Q50C before and after incubation with GNPs was found to correlate with the amount of bound CVN $^{Q50C}$ . The binding constants,  $K_{d1}$  (Domain A) and K<sub>d2</sub> (Domain B), of the monomeric glycan (M2 or M3) and CVN Q50C were measured through isothermal titration calorimetry (ITC). The binding affinities between the GNPs and  $\text{CVN}^{\circ 50C}(K_{D1} \text{ and } K_{D2})$  were then obtained from the best-fitting

curves using a two-site competitive binding model with the modified Cheng–Prusoff equation<sup>36</sup>:

$$f = 1 - \frac{f_{Bmax1}}{1 + \frac{K_{D1}}{[GNP - M2]} \left(1 + \frac{[M2]}{K_{d1}}\right)} - \frac{f_{Bmax2}}{1 + \frac{K_{D2}}{[GNP - M2]} \left(1 + \frac{[M2]}{K_{d2}}\right)}$$

The GNPs exert multi-fold affinity enhancement compared to free monomeric mannose (M2 or M3) when their binding constants towards CVN<sup>Q50C</sup> were measured (Table 2).

Nolting et al employed Biotin NeutrAvidin Adhesion Assays (BNAA) to screen GNP drug candidates against HIV-associated glycoprotein, gp120, that binds galatcosylceramide (GalCer), a glyco-sphingolipid receptor on mucosal cells. <sup>37</sup> In this assay, a NeutrAvidin coated plate was incubated with biotinylated GalCer (bGalCer) to generate a GalCer monolayer. Following monolayer generation, horseradish peroxidase-recobinant gp120 (HRP-rgp120) of fixed amount (0.333 µg) was added. Saturated binding of HRP-

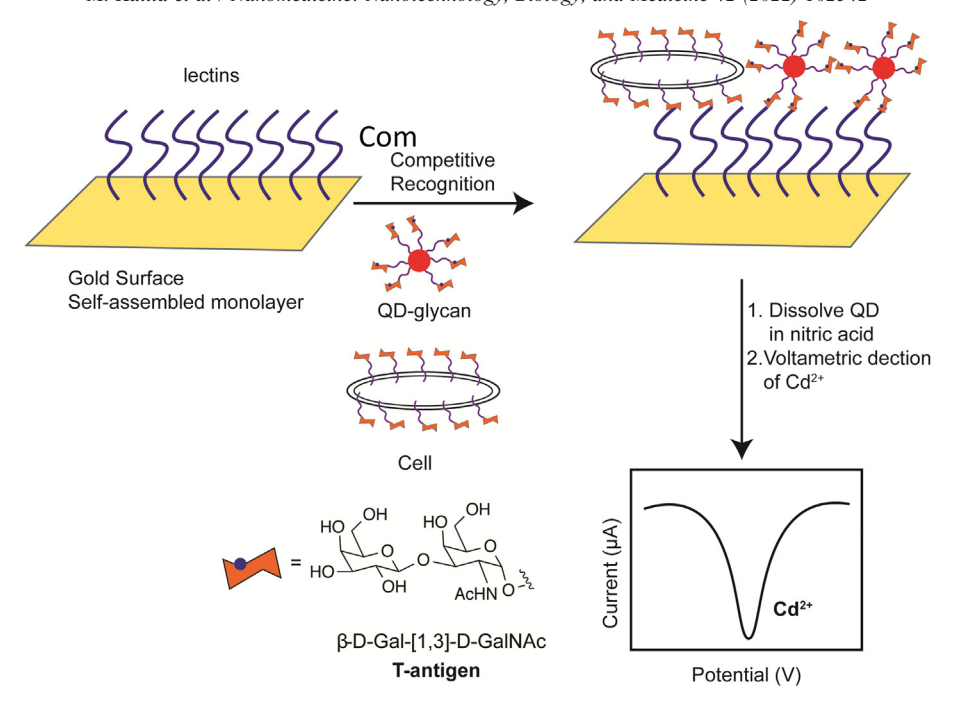


Figure 4. Electrochemical assay for glycan measurement. The electrochemical assay starts with a self-assembled monolayer (SAM) of lectins on gold surface. Next, CdS-glycans and breast cancer's T antigens compete for SAM of lectins. Finally, nitric acid dissolved CdS QDs to produce a solution containing Cd<sup>2+</sup> for anodic stripping voltammetric detection of the cell surface T-antigen. Redrawn from Ref. [21].

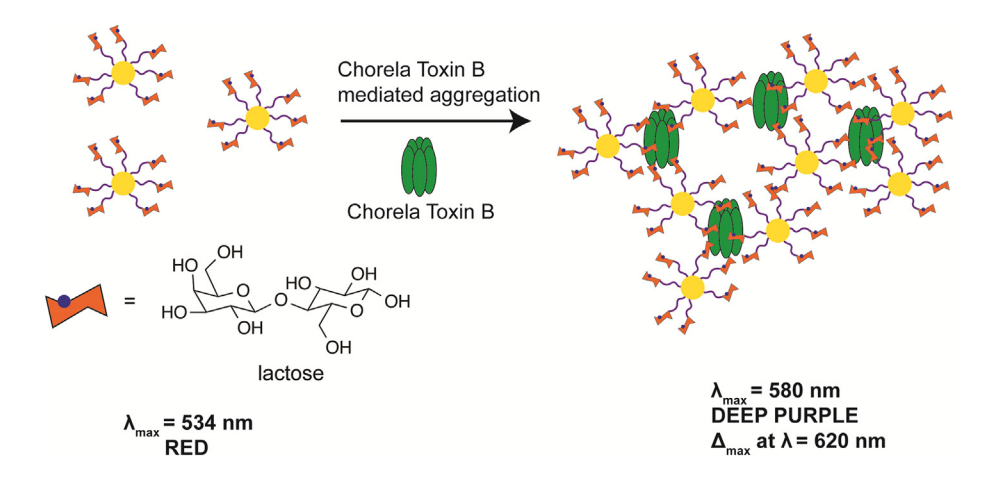


Figure 5. Colorimetric assay for glycan sensing. The cholera toxin, AB<sub>5</sub> hexameric protein (CTB) binds the pentasaccharide residue of the GM1 ganglioside in the small intestine. The Au-lactose mimics the pentasaccharide. The CTB mediates Au-lactose aggregation, broadens the surface plasmon absorption band ( $\lambda$  = 534 nm) and shifts the color of solution from red to deep purple ( $\lambda$  = 580 nm). Redrawn from Ref. [29].

rgp120 with GalCer produced maximum absorbance at  $\lambda_{max}=630$  nm  $\it via$  chemiluminescence. Addition of serially diluted GNPs/free ligands (galactose, glucose) (1-400 µg/mL) resulted in competition for biotinylated GalCer epitopes and replaced HRP-rgp120 from the plate (Figure 7). Finally, the plate was rinsed off and absorbance at  $\lambda_{max}=630$  nm was recorded. This absorbance correspoded to unreplaced HRP-rgp120 (bound to bGalCer) which remained on the plate. The degree of competition for GalCer epitopes was monitored by measuring plate absorbances every minute for 20 min. A plot of HRP-rgp120 bound to bGalCer (%) vs GNPs/free ligands concentration (mM) furnished EC50 values for each analyte.

The GNPs display multivalent galactosyl and glucosyl headgroups, a presumed condition for enhanced binding ability. Indeed GNPs (with ~120 glycans/gold nanoparticle) asserted significantly higher activity compared to free congeners, 450 times for gold-galactosyl and >300 times for gold-glucosyl ligands. Thus, polyvalent presentation of glycans on gold nanoparticles enhances the avidity for recobinant gp120. The BNAA assay can be a model for future studies to discover antiviral drugs.

Baker et al developed a nitrocellulose paper-based lateral flow detection (LFD) system involving AuNP conjugated *N*-acetyl neuraminic acid (NeuNAc) and its derivatives. <sup>38</sup> The FLD

Table 1 Lectins and their glycan ligands. 31–33

| Lectins                            | Origin               | Glycan ligand  |
|------------------------------------|----------------------|--|
| Concanavalin-A (ConA)              | Canavalia ensiformis | Terminal α Man, Man α3[Man α6] Man   |
| Dolichos biflorus agglutinin (DBA) | D. biflorus          | GalNAc α(1,3) GalNAc/Gal   |
| Peanut agglutinin (PNA)            | Arachis hypogaea     | Gal β(1,3)GalNAc, Terminal β-Gal   |
| Wheat germ agglutinin (WGA)        | Triticum unlgari     | (Neu5Ac) (Gal β4GlcNAc) <sub>1-3,4</sub> (GlcNAc β4GlcNAc) <sub>1-3,4</sub>      |
| Soybean agglutinin (SBA)           | Soybean              | Terminal α-GalNAc, Tn antigen  |
| Lotus tetragonolobus lectin (LTL)  | Lotus tetragonolobus | Fuc $\alpha(1-3)$ (Gal $\beta$ 1-4)GlcNAc, Fuc $\alpha$ 1-2Gal $\beta$ 1-4GlcNAc |

Man, mannose; GalNAc, N-acetylgalactosamine; Gal, galactose; GlcNAc, N-acetylglucosamine; Neu5Ac, N-acetylneuraminic acid; Fuc, fucose.

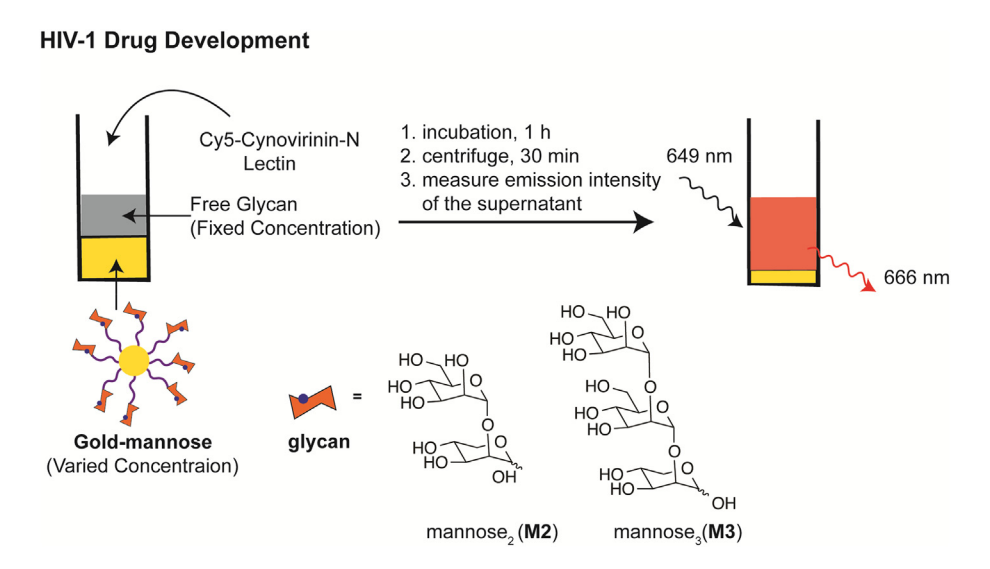


Figure 6. HIV-1 drug development. Gold-low molecular weight mannoses (GNP-M2 or GNP-M3) compete with free glycans (M2 or M3) in presence of Cy5-cyanovirin-N (CV-N). The samples were shaken, centrifuged, and separated from nanoparticles pallets. Binding constants between GNP and CVN $^{Q50C}$ ,  $K_{D1}$  and  $K_{D2}$  were calculated by using modified Cheng–Prusoff equation.

Table 2 Binding constants of glyconanoparticles (GNPs) and their ligands for Cyanovirin-N (CV-N).

| Ligands | $K_{d1}$ or $K_{D1}$ (domain A) | K <sub>d2</sub> or K <sub>D2</sub> (domain B) |
|---------|---------------------------------|---|
| M2      | $700 \pm 50 \ \mu M$            | $64 \pm 4 \mu M$                              |
| GNP-M2  | $56.4 \pm 7 \text{ nM}$         | $0.24 \pm 0.1 \text{ nM}$                     |
| M3      | $3.4\pm0.2~\mu M$               | $43 \pm 2 \ \mu M$                            |
| GNP-M3  | $0.011 \pm 0.007 \text{ nM}$    | $11.8 \pm 2.3 \text{ nM}$                     |

demonstrated that NeuNAc bound SARS-COV-2 spike glycoprotein as well as detected the spike glycoprotein of the SARS-COV-1 in 30 min. In this study, the recombinant S1 subunit (SARS-COV-2,S1) spike protein was immobilized onto sensors and AuNP conjuagtes flowed over them. Among all AuNP conjugates the NeuNAc-AuNPs demonstrated stronger affinity when compared to sialyllactose isomers ( $\alpha 2,3/\alpha 2,6$ ) for SARS-COV-2,S1, and detected the spike protein at <8 nM. In an alternative dipstick sandwich study, the analyte was added to the AuNP solution instead of drying onto the nitrocellulose paper. A coronavirus mimic was developed by decorating SARS-COV-2, S1 spike glycoprotein on 100 nm polystyrene nanoparticles sandwiched between NeuNAc-anchor protein (bovine serum albumin) and NeuNAc-AuNP solution. This device detected the

coronavirus mimic at a concentration of 5 nM protein. The cost-effective AuNP biolayer interferometry platform detected SARS-COV-2,S1 within 30 min opening a window for its widespread use.

In a subsequent study, Baker et al exploited the S1 spike protein–glycan interaction to develop a low-cost flow-through device that can detect SARS-COV-2. The S1 spike protein of the SARS-COV-2 binds the terminal sialic acid ( $\alpha$ -N-acetyl neuraminic acid) containing receptor such as angiotensin-converting enzyme 2 (ACE2), mediates the viral entry into a cell, and controls its genetic machinary.

Briefly, the flow-through device is composed of the sample addition to the nitrocellulose strip, the flow of the sialic acid—gold nanoparticles *via* running buffer, and final detection with silver staining. The final step involved gold nanoparticles catalyzing the reduction of water-soluble silver ions into insoluble metallic silver. This method improved the detection limit. In flow-through assay, the authors replaced the positive testline (SARS-COV-2, S1) with the primary sample (nasal swabs) and validated the results with RT-PCR, resulting in 85% sensitivity and 93% specificity (at RT-PCR cycle threshold, Ct = 25).

This flow-through device also reliably detected recombinant mutant truncated spike proteins – B1.1.7, B.1.351, and P1 (variants first detected in Kent (U.K.), South Africa, and Brazil) – expressed in

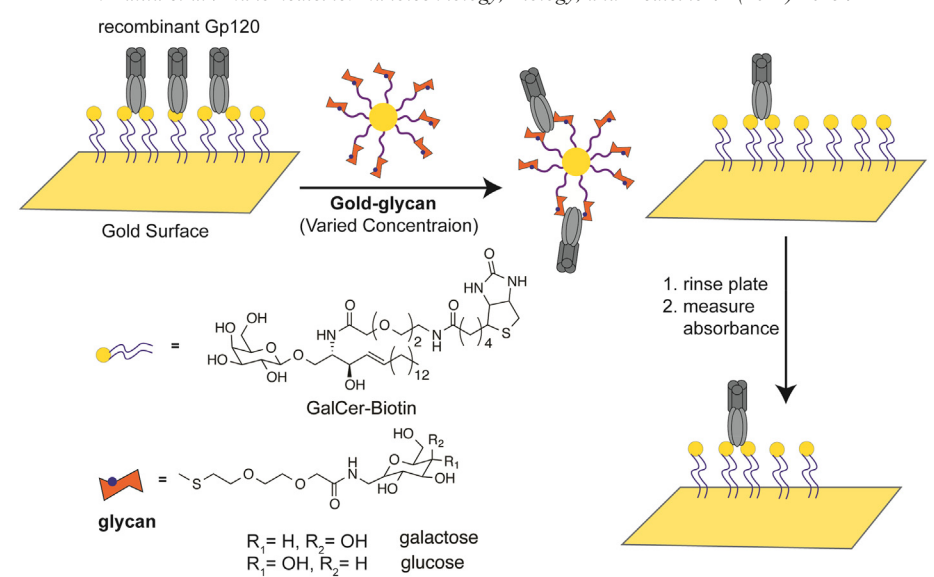


Figure 7. Biotin NeutrAvidin Adhesion Assay (BNAA). NetrAvidin coated plate was incubated with biotin-galactosylceramide (bGalCer). This follows incubation with horseradish peroxidase-recombinant gp120 (HRP-rgp120). Serially diluted galactose- and glucose-glyconanoparticles (GNPs) displaced HRP-rgp120. Finally, the plate was rinsed off. The efficacy of replacement and binding strength between GNPs and HRP-gp120 were determined *via* the chemiluminescence of HRP-gp120.

 $E.\ coli.$  The main criticism of this study is the low detection limit of  $\sim 10$  transduction units/device (1  $\mu L$  of the lentiviral solution). This may be, in part, due to the detection of inert (nontransducible) particles which also bear the spike protein. Nevertheless, this glyconanotechnology based COVID-19 test can improve the rapid testing problems in countries around the world.

To map structurally diverse heparan sulfate (HS) epitopes conjugated quantum dots (QD) with antithrombin III (AT) and FGF2, proteins were used to generate QD-AT and QD-FGF2 probes. 40 These two probes revealed abundance and distribution of rare anticoagulant 3-O-sulfated pentasaccharide and ubiquitous 2-O-sulfated tetrasaccharide motifs of HS in endothelial cells and aortic tissue sections with excellent resolution. 40 When a QD-AT probe was applied in the aorta of two age groups (two-weeks and six-months) the six-month-old group showed a 79-fold decreased fluorescence of the QD-AT probe. This study demonstrated the utility of QD-AT (and QD-FGF2) in identifying age-associated changes in HS motifs. The technology for rare HS motifs may be useful in pinpointing risk factors such as age-associated thrombosis and neurodegeneration 41,42 (Figure 8).

Chuang et al investigated the carbohydrate-protein binding constant using gold nanoparticle-glycans (Au-glycans) and concanavalin A lectin.  $^{43}$  The concanavalin A mediated Au-glycan aggregation induces a change in the surface plasmon resonance of AuNP. A plot of the AuNP absorbances (Y axis) against titrating concentrations of concanavalin A (X axis) generated the dissociation constant ( $K_d$ ) upon non-linear curve fitting. The authors reported the decreasing order of  $K_d$  for the binding between carbohydrates with concanavalin A: maltose > mannose > glucose > lactose.

Kikkeri et al synthesized Au-sialic acid derivatives and QD-sialic acid binding proteins (SBPs) to determine sialic acid compositions and their glycosylation linkages ( $\alpha$ 2-6 versus  $\alpha$ 2-3). <sup>44</sup> This work

exploited gold nanoparticles' nanometal surface energy transfer (NSET). The AuNPs exerted NSET on QD-SBPs and quenched QD fluorescence within ~10 nm distance. Titration with external sialic acids displaced weak SBP-sialic acid interactions, disrupted the NSET, and restored concentration-dependent QD fluorescence from the QDs. The fluorescence quenching efficiency was quantified by the Stern–Volmer equation <sup>45,46</sup>:

$$F/F_0 = 1 + K_{SV} [AuNP]$$

 $F_0$  and F are the steady-state fluorescence intensities in the absence and presence of the AuNPs, respectively.  $K_{\rm SV}$  is the Stern–Volmer quenching constant, which was used to generate four NSET pairs of Au-sialic acid and QD-SBP. Next, addition of external sialic acids broke each NSET pair. A plot of  $F/F_0$  (Y-axis) and titrating concentrations of external sialic acids (X-axis) furnished a library of calibration plots. Finally, these plots informed the identity of the biological samples (mouse plasma, bovine submaxillary mucin (BSM), de-O-acetylated (D-BSM), and porcine submaxillary mucin (PSM) solutions).

## Quality control

The peptidoglycans on bacterial cell walls summon glycans on mammalian cells and initiate infection. <sup>47</sup> El-Boubbou et al designed mammalian cell membrane mimic D-mannose (and D-galactose) stabilized iron oxide (Fe<sub>3</sub>O<sub>4</sub>)-Silica core-shell magnetic nanoparticles (MGNP) that detected *E. coli* within 5 min, decontaminated up to 88% of bacteria from the medium, and distinguished three different *E. coli* strains. <sup>48</sup>

Incubation of MGNPs with *E. coli* (10<sup>3</sup>-10<sup>7</sup> cells/mL in PBS buffer) for 5 min produced effective D-mannose interaction with the bacterial cell wall. A magnetic field separated the MGNP-*E. coli* aggregates in the solution. The aggregates were removed,

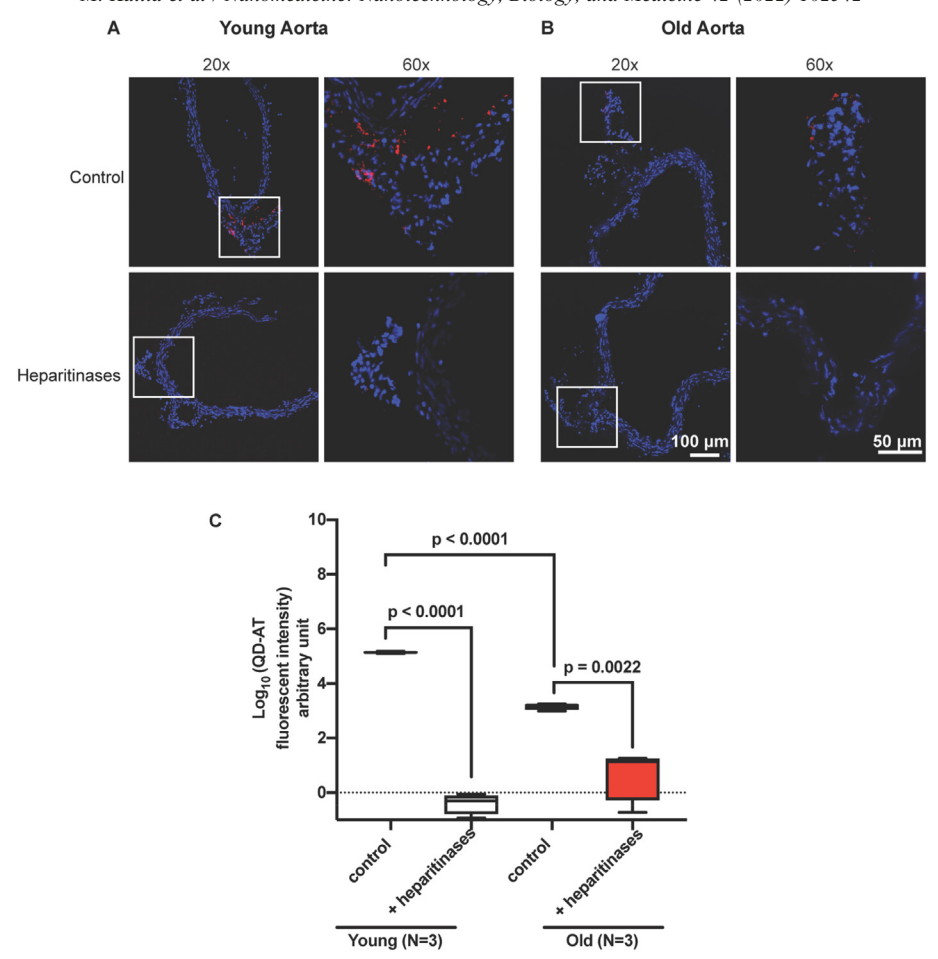


Figure 8. QD-antithombin probe pinpoints age-dependent 3-O-sulfated heparan sulfate. QD-AT staining of mouse aorta to image 3-O-sulfated heparan sulfate (3-OS-HS) in (**A**) control young aorta, heparitinases treated young aorta, and (**B**) control old aorta and heparitinases treated old aorta. (**C**) There is about 79-fold reduction in the fluorescence intensity of QD-AT staining (red) as aorta gets older from two weeks to six months (N = 3 mice, four different 20× cryosection images) (P < .0001), suggesting significant reduction in the anticoagulant HS structures. (Scale bar = 100  $\mu$ m for 20×, 50  $\mu$ m for 60×, red = QD-AT, blue = DAPI).

washed, stained with a fluorescent dye, and imaged under microscope.

MGNP-mannose and MGNP-galactose were deployed to delineate different strains of *E. coli* based on their protein-glycan binding strength: ORN178 (mannose strong, galactose weak), ORN208 (mannose weak, galactose weak), and ES (mannose strong, galactose strong). For example, MGNP-mannose captured 65% of ORN178, while MGNP-galactose caught only 15%. These multi-functional MGNPs could potentially find clinical applications.

We reported a gold-heparin-dye nanosensor for ultrasensitive detection of over-sulfated chondroitin sulfate (OSCS) contaminant (10<sup>-9</sup>% w/w) in pharmaceutical grade heparin. <sup>23</sup> Such contamination was responsible for the death of approximately 150 people around the world in 2008. In developing this technology, we leveraged gold nanoparticles' efficient quenching of dye fluorescence (through NSET) and OSCS contaminant's inhibition of the heparitinase enzyme. In the absence of OSCS contaminant, the heparinase enzyme digested nanosensor's heparin-dye ligands, released oligosaccharide-dye fragments from the gold's surface, and restored dye fluorescence. However,

the OSCS contaminant in heparin suppressed this recovery through heparitinase inhibition. Titration with OSCS produced concentration dependent fluorescence reduction. This technology shall aid the regulatory bodies in detecting life-threatening OSCS contaminant in life-saving heparin (Figure 9).

#### **Diagnostics**

Glycans stabilize the surface of nanoparticles such as iron oxide, gold, and quantum dots and supply biocompatibility, multi-valency, and functional affinity to target biological samples: cells, tissues, or organs. The nanoparticles provide signal output of magnetic resonance (MR) and fluorescence. This section reviews glyco-nanotechnology of these nanoparticles in various biological samples.

#### Glyco-magnetics

Glyco-magnetics have two parts: glycans and magnetic resonance active nanoparticles. Glycans target the biological sample of interest mainly *via* glycan–receptor interactions. MRI-

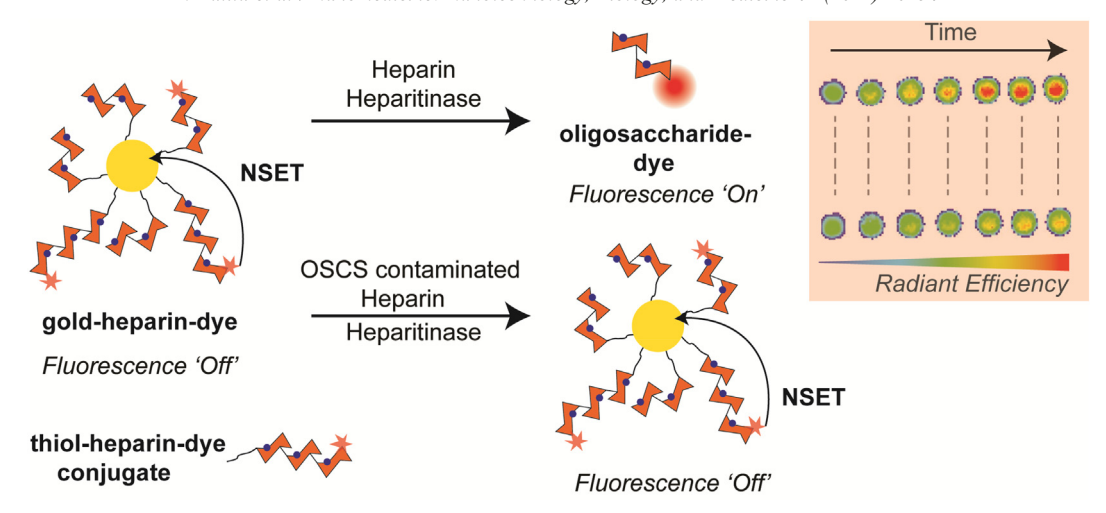


Figure 9. Heparin quality control. Oversulfated chondroitin sulfate (OSCS) contaminant in heparin was detected by gold-heparin-dye, a NSET nanoprobe. Heparitinase enzymes cleaved off dye labeled heparin polysaccharides into smaller oligosaccharide-dye, broke the NSET, and restored the dye fluorescence. The OSCS contaminant inhibited the heparitinase enzymes, resisted the heparin cleavage, and kept the fluorescence "off". Serially diluted OSCS showed regular increase in the dye fluorescence.

Figure 10. Iron oxide-glycans image brain pathology. Iron oxide-sialyl Lewis targets activated E- and P-selectin in rat brains revealing brain pathology via MRI.

active nanoparticles can be used to produce  $T_1$  (longitudinal relaxation time) and  $T_2$  (transverse relaxation time) weighted maps of the target biological sample. <sup>49,50</sup>

Imaging of brain disease with sialyl Lewis<sup>X</sup>-iron oxide

Acute inflammation or injury triggers upregulation of carbohydrate binding transmembrane proteins E-selectin (CD62E) and P-selectin (CD62P) on endothelial cells. <sup>51</sup> This event mobilizes leucocytes with sialyl Lewis<sup>X</sup> (sLe<sup>x</sup>) on their cell membranes towards the site of inflammation. To visualize E-/P-

selectin endothelial markers in neurological disease models, van Kasteren et al synthesized MRI active sialyl Lewis (sLe\*) decorated iron oxide nanoparticles. The synthesis involved two steps: first, amine (-NH<sub>2</sub>) terminated dextran ligands furnished amine-functionalized iron oxide nanoparticles displaying 10<sup>5</sup> to 10<sup>7</sup> -NH<sub>2</sub> groups for subsequent sLe\* conjugation. Second, -NH<sub>2</sub> functionalized iron oxide nanoparticles reacted with 1-thio-2-imido-2-methoxy-ethyl (S-CH<sub>2</sub>-C(NH)OMe) group at the anomeric carbon of sugar resulting in mono-, di-, tri-, and tetra-saccharides (sLe\*) on their surface (Figure 10).

## Fe<sub>3</sub>O<sub>4</sub>/SiO<sub>2</sub> core/shellsialic acid (of GM1 ganglioside)

Figure 11. The Fe<sub>3</sub>O<sub>4</sub>/SiO<sub>2</sub>-sialic acid core-shell nanoparticle binds  $\beta$ -amyloid aggregates *via* GM1 ganglioside (sialic acid containing glycosphangolipid), reduces the T<sub>2</sub>\* relaxation time, and detects 0.05  $\mu$ M  $\beta$ -amyloid in in vitro. Redrawn from Ref. [14].

The interleukin-1 $\beta$  (100 ng) microinjection activated the E-/P-selectin in the left striatum of a rat's brain. Three hours later, systemic injection (10 ng) of sLe<sup>x</sup>-iron oxide nanoparticles created a biodistribution map through a 3D gradient echo T<sub>2</sub>\* pulse sequence. MRI images confirmed localization of sLe<sup>x</sup>-GNPs at the left cranial hemisphere. This study also examined other brain pathological conditions such as focal MS like lesions and endothelin-induced focal strokes.

## Iron oxide-silica core-shell binds $\beta$ -amyloid plaque

Iron oxide (Fe<sub>3</sub>O<sub>4</sub>)-silica (SiO<sub>2</sub>) core-shell nanoparticles diagnosed ischemic brain (stroke) and  $\beta$ -amyloid plaques via glycan ligands on the nanoparticles. <sup>14</sup> Sialyl Lewis (sLe\*) targeted overexpressed E and P selectin transmembrane protein on injured endothelial of the brain (Figure 11). The sLe\*-Fe<sub>3</sub>O<sub>4</sub>-SiO<sub>2</sub> core-shell nanoparticle appeared to cross the blood–brain barrier, labeled the injured blood vessels, and can be used to construct a  $T_2$ \* weighted map of brain ischemia. This study cautioned that the in vivo results were inconclusive as sLe\* nanoparticles induced selectin upregulation in the entire brain while control nanoparticles without sugar showed the best contrast.

The same paper reported sialic acid-  $Fe_3O_4$ -SiO<sub>2</sub> core-shell nanoparticles binding  $\beta$ -amyloid aggregates. The construct was inspired by GM1 ganglioside – a sialic acid containing glycosphangolipid – that binds and mediates  $\beta$ -amyloid aggregates. After binding  $\beta$ -amyloid, the sialic acid  $Fe_3O_4$ -SiO<sub>2</sub> reduced the  $T_2*$  relaxation time from 23 ms to 16 ms and the corresponding map detected 0.05  $\mu$ M  $\beta$ -amyloid in vitro. The nanoparticle also catalyzed the  $\beta$ -sheet rich fibril formation and protected the neurons from cytotoxicity. Future studies could construct nanoparticles for improved blood brain barrier permeation and specific labeling of the disease site.

#### MRI finger printing cancers

Various glycans – mannose, galactose, fucose, sialic acid, and *N*-acetylglucosamine – immobilized on paramagnetic Fe<sub>3</sub>O<sub>4</sub> nanoparticles bind cancer cell associated lectins (carbohydrate binding proteins)<sup>53</sup> (Figure 12). The binding affinity depends on the type and abundance of lectins on cancer cells (Table 1). Overexpressed lectins on cancer cells induced GNP aggregation, reduced the relaxation time, and enhanced the signal to noise ratio. A library of glycan-Fe<sub>3</sub>O<sub>4</sub> nanoparticles generated T<sub>2</sub>\* weighted MRI fingerprint maps of various cancers such as kidney cancer (A498), lung cancer (A549), colon cancer (HT29),

ovarian cancer (SKOV-3), meta-static mouse melanoma (B16-F10), and less metastatic mouse melanoma (B16-F1).

## Gold-gadolinium hybrid detects glioma

Marradi et al imaged glioma via a hybrid gold nanoplatform consisting of glucose and DO3A-Gd. <sup>54</sup> Gold provides a platform for sugar molecules and tetraazacyclododecane triacetic acid (DO3A), a chelator of gadolinium (III). The longitudinal relaxation time ( $T_1$ ) of Gd(III), a paramagnetic probe for MRI, is a function of sugar chirality (glucose, galactose or lactose) and the distance between sugar and Gd(III) (Figure 13).

#### Hyaluronic acid-iron oxide maps atherosclerosis

Superparamagnetic  $Fe_3O_4$  nanoparticles labeled with <u>hyaluronic acid</u> targets elevated CD44 receptors in the atherosclerosis plaques consisting of vascular endothelial cells, macrophages, and smooth muscle cells. During inflammation, cytokine TNF- $\alpha$  installs sulfate group on CD44, changes its conformation, and enhances its affinity for hyaluronic acid. Fe sulfated CD44's high affinity for hyaluronic acid produced rapid and selective binding, and required low concentration of nanoparticles to generate  $T_2^*$  weighted MR images of the plaques (Figure 14, A).

## Magneto-opto glyco-nanotechnology

Glycan stabilized magneto-opto nanoparticles reported both magnetic resonance and fluorescence at the disease site. Galactosyl-Fe<sub>3</sub>O<sub>4</sub>-Cyanine 3 bound asialoglycoprotein receptor (ASGPR) on liver cancer cells (HepG2) underwent receptor-mediated endocytosis and accumulated in the late endosome and/or lysosomes. This dual probe recorded MRI, through Fe<sub>3</sub>O<sub>4</sub>, and fluorescence, through Cyanine 3 dye, to diagnose HepG2 cancer. Control HeLa cells without receptor showed no signal in in vitro studies. The receptor affinity increased with glycan valency with trivalent galactose displaying optimal spatial orientation for ASGPR binding. <sup>59</sup>

Lactose modified nanoparticles (<u>lactose</u>-gold-Fe $_3$ O $_4$ -Texas Red) also targeted cervical carcinoma cells (C33), internalized rapidly (20-30 min) through caveolae mechanism, and reported MR and fluorescence. A gold shell around Fe $_3$ O $_4$  core protected the magnetic core from oxidation, supplied biocompatibility, and provided sites of bioconjugation.

## Activated macrophage through hyaluronic acid-Fe<sub>3</sub>O<sub>4</sub>

Hyaluronic acid (HA) (only non-sulfated glycosaminoglycan) synthesized at the inner plasma membrane exits into the extracellular matrix. Kamat et al reported HA functionalized paramagnetic Fe<sub>3</sub>O<sub>4</sub> nanoparticles to construct an MRI map of activated macrophages during inflammation and injury. <sup>60</sup> The nanoprobe targeted upregulated CD44, a hyaluronic acid binding transmembrane receptor on activated macrophages, which are recruited to the site of inflammation (Figure 14, A).

Confocal images confirmed the accumulation of HA-Fe<sub>3</sub>O<sub>4</sub> nanoprobes at the nucleus of human monocytic cell line THP-1, making them potential drug delivery vehicles.

#### Glyco-gold

In this section, we will discuss glycan decorated gold nanoparticles. Two examples involve generic gold-glycan-dye nanoprobes. These probes rely on gold nanoparticles' ability to

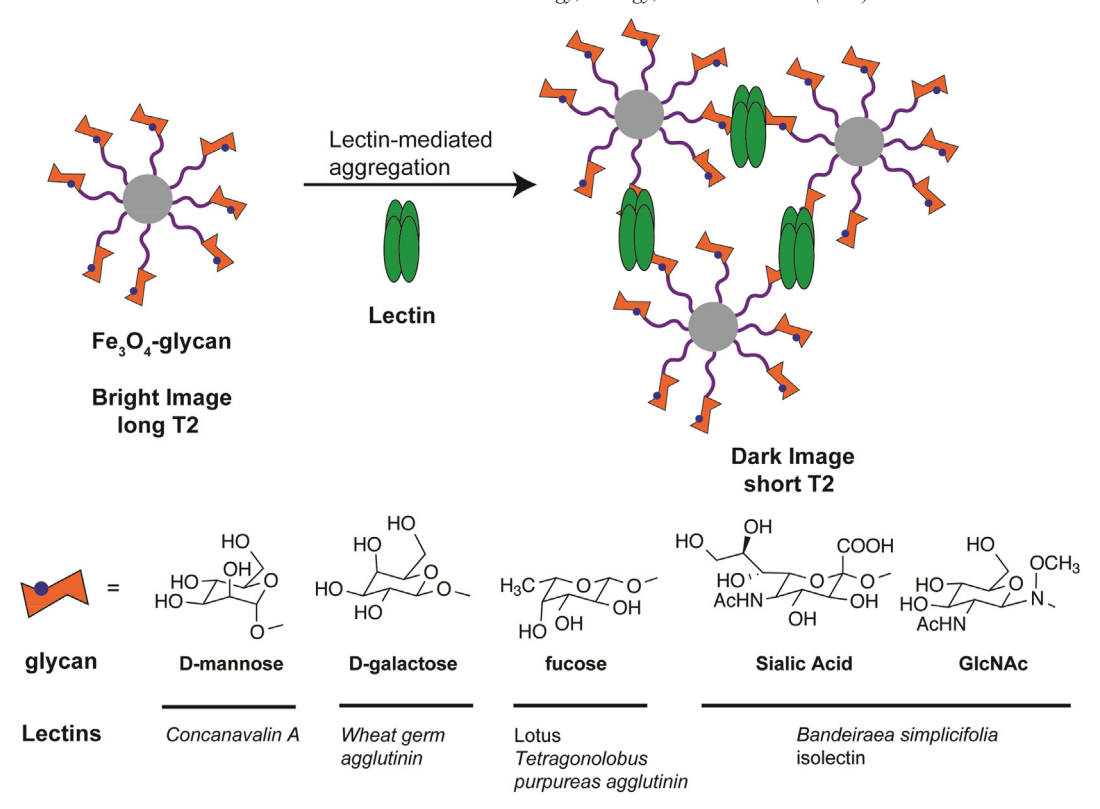


Figure 12. Overexpressed lectins on cancer cell surface mediate nanoparticle aggregation, reduce the relaxation time, and enhance the signal to noise ratio of T<sub>2</sub> weighted images. Redrawn from Ref. [53].

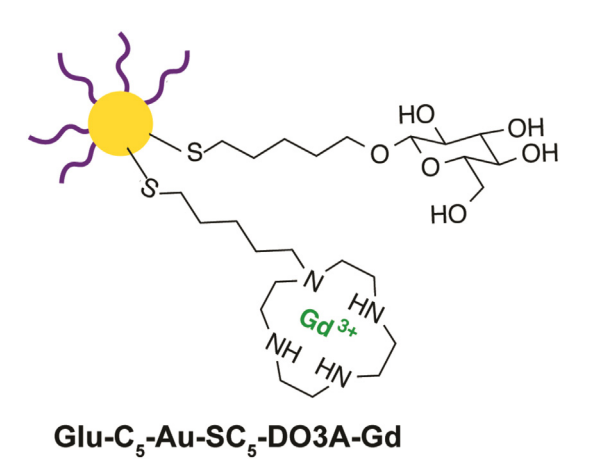


Figure 13. AuNP stabilized with glycans and linked to tetraazacyclododecane triacetic acid (DO3A)—a chelator of MRI active gadolinium (III) detects glioma through MRI. Redrawn from Ref. [54].

quench dye fluorescence through nanometal surface energy transfer (NSET) mechanism and dysregulated glycan-degrading enzymes' (biomarker of pathology) tolerance for these synthetic substrates in their active sites. When these two criteria are met, gold-glycan-dye probes could report the dysregulated enzyme activity through fluorescence enhancement. Mechanistically, the dysregulated enzyme cleaves off the polysaccharide chain, releases oligosaccharide-dye fragments from the surface of gold, and breaks the NSET. These events restore the fluores-

cence of the dye and correlate enzyme activity with disease diagnosis.

Finally, we will discuss glyco-gold-nanoPET involving PET active <sup>68</sup>Ga and blood brain barrier permeable glucose.

## Gold-hyaluronic acid-dye

Gold-hyaluronic acid-near infrared dye sensed deep tissue rheumatoid arthritis and metastatic cancer biomarkers such as reactive oxygen species (ROS) (limit of detection 0.2 μM) and the hyaluronidase enzyme (limit of detection 1 unit/mL). <sup>15</sup> The nanoprobe's fluorescence was 'off' due to the NSET phenomenon. Hyaluronidase enzymes cleaved hyaluronic acid, released oligosaccharide-dye fragments from gold nanoparticles, and switched 'on' the fluorescence. The fluorescence enhancement correlated with ROS/hyaluronidase concentration. The nanoprobe detected arthritis within six hours post-intravenous injection with 5.1-fold increase in fluorescence signal over control mice. And the probe identified human ovarian cancer (OVCAR-3) within four hours post-injection with 6.1-fold signal enhancement over control.

## Gold-heparin/RGD-dye

Heparin-dye (HiLyte-Fluor 647) immobilized on gold nanoparticles identified the extracellular matrix of metastatic cancer that secreted heparinase enzyme. The enzyme cleaved off heparin polysaccharide into shorter oligosaccharides and switched on the fluorescence of the dye with 2.6 to 5.5-fold fluorescence recovery<sup>61</sup> (Figure 14, *B*). Additional conjugation of the gold nanoplatform, with thiol capped polyethylene glycol-

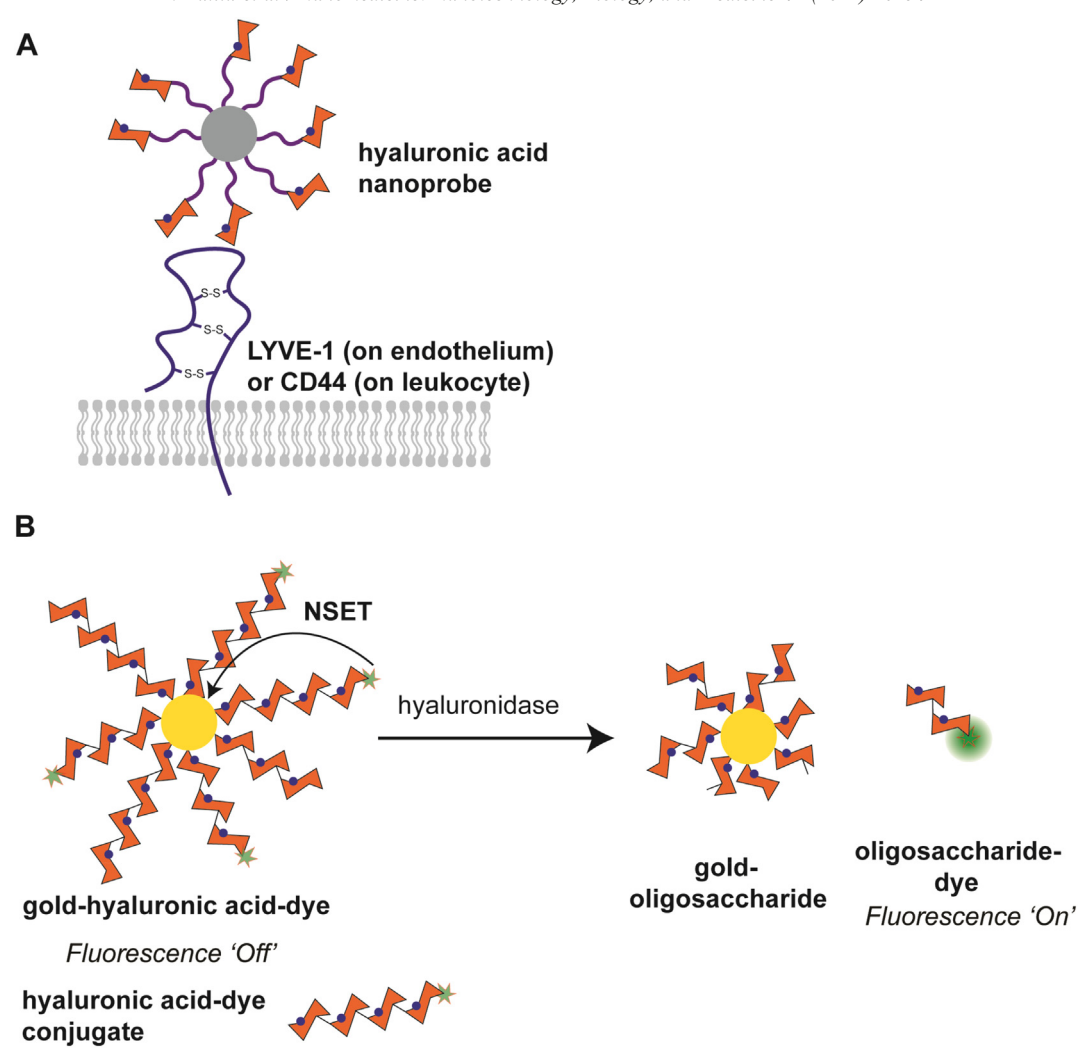


Figure 14. Hyaluronic acid based nanoprobes. (A) HA nanoprobe binds LYVE-1 receptors on endothelium and reveals lymphatic vessel formation during cancer progression (Bhang SH, Won N, Lee T-J, et al. Hyaluronic acid-quantum dot conjugates for in vivo lymphatic vessel imaging. ACS Nano. 3(6), 1389–1398 (2009)). Inflammation upregulates CD44 expression on activated macrophages. HA nanoprobe identifies the CD44 and tracks activated macrophages (Kamat M, El-Boubbou K, Zhu DC, et al. Hyaluronic acid immobilized magnetic nanoparticles for active targeting and imaging of macrophages. Bioconjug. Chem. 21(11), 2128–2135 (2010)). (B) Gold-hyaluronic acid-dye probe assays hyaluronidase enzyme activity—a hallmark of rheumatoid arthritis and metastatic cancer. The fluorescence of the dye is 'off' before enzymatic cleavage due to nano-surface energy transfer (NSET) from the dye to gold nanoparticles. The hyaluronidase enzyme cleaves the nanoprobe, releases oligosaccharide-dye fragments, and switches 'on' the dye fluorescence by breaking the NSET phenomenon.

RGD ligand, targeted metastatic cancer through RGD mediated  $\alpha_v\beta 3$  integrin interaction. <sup>61,62</sup> Cell surface assisted endocytosis of these nano-conjugates triggered apoptosis demonstrating the therapeutic potential of Au-Heparin/polyethylene glycol-RGD. <sup>61</sup>

## Gold-68Ga nano-PET

Positron emission tomography (PET) active gold nanoparticles (AuNP) were used to evaluate their permeability through the blood–brain barrier (BBB). The AuNPs (2 nm diameter), stabilized with glucose, were decorated with BBB-permeable opioid neuropeptides and a cyclic chelator of the positron emitter <sup>68</sup>Ga (1,4,7-triazacyclono-nane-1,4,7-triacetic acid (NOTA)) to determine in vivo biodistribution. <sup>63</sup> The Leu-enkephalin peptide (Enk) labeled <sup>68</sup>Ga-AuNPs increase BBB crossing approximately 3-fold compared to control <sup>68</sup>Ga-AuNPs. The authors reasoned that glucose imparted biocompatibility to AuNPs and

improved their BBB penetration due to the brain's glucose addiction.

## Glyco-quantum dots

When compared with traditional organic dyes, quantum dots are 20 times brighter, are 100 times more stable against photobleaching, and have only one-third the spectral linewidth. <sup>64,65</sup> These qualities of quantum dot labeled glyconanoparticles have improved the sensitivity for diagnosis of biomarkers.

#### Liver cirrhosis through hyaluronic acid-QD conjugates

Alcohol or dimethylnitrosamine induced liver cirrhosis results in over production of hyaluronic acid in the serum and overexpression of CD44 receptors on injured hepatic cells. <sup>16</sup> A hyaluronic acid-QD probe was constructed by labeling near

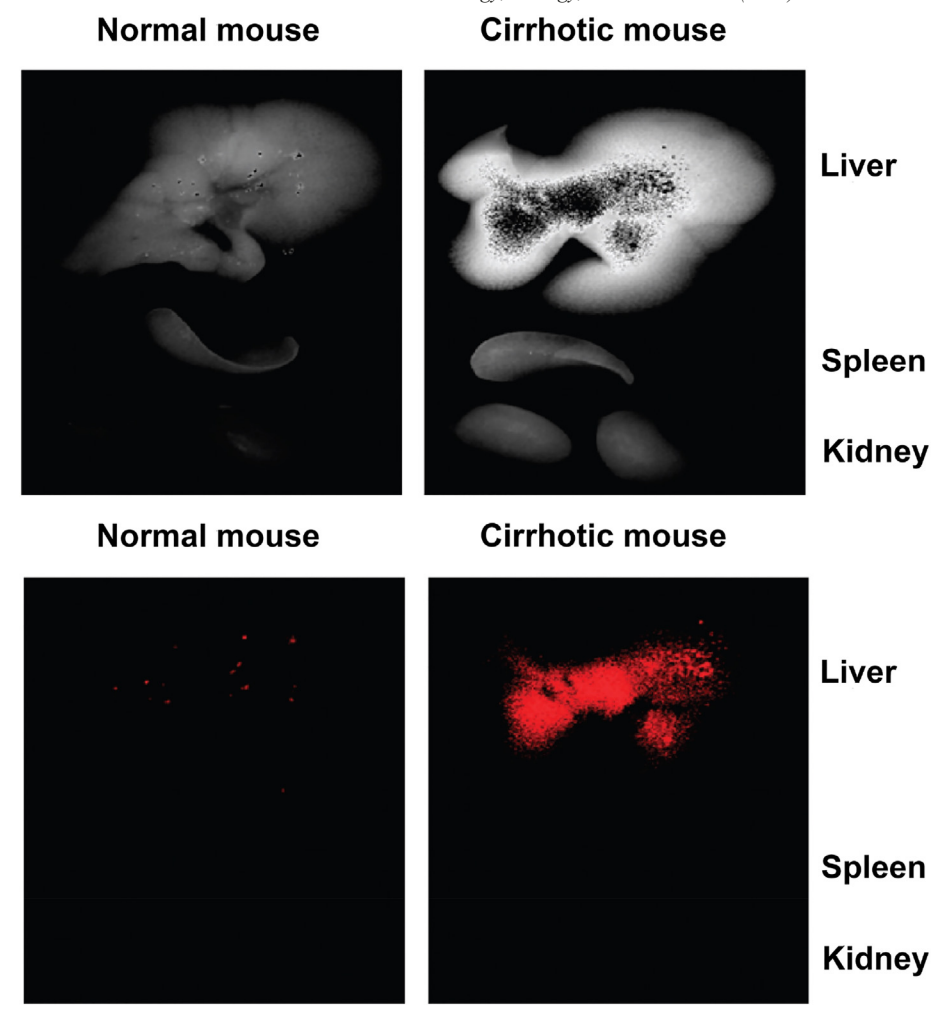


Figure 15. "(A) Autoexposed fluorescent images of dissected livers (top), spleens (middle), and kidneys (bottom) 3 days after tail-vein injections of hyaluronic acid—quantum dot (HA-QDot) conjugates to normal and cirrhotic mice. (B) Fluorescent images of (A) at a detection wavelength of 790 nm." With permission from Kim KS, Hur W, Park S-J, et al. Bioimaging for targeted delivery of hyaluronic acid derivatives to the livers in cirrhotic mice using quantum dots. *ACS Nano.* 4(6), 3005–3014 (2010)), copyright American Chemical Society, Washington, DC, 2010.

infrared QD (emission wavelength 800 nm) with adipic acid dihydrazide modified HA (~22% modification of the hyaluronic acid chain) to target CD44 of damaged liver cells (Figure 15). Indeed, the hyaluronic acid-QD probe showed better homing and longer residence period (up to 8 days) in the cirrhotic liver than in normal liver of BALB/c mice. The success of real-time bioimaging of liver disease through hyaluronic acid decorated QD can be further exploited for targeted drug delivery.

#### Lymphatic vessel formation

During cancer progression, expression of LYVE-1 receptor is upregulated in lymphatic endothelial cells (LEC). <sup>66,67</sup> Since LYVE-1 is a hyaluronic acid binding protein, <u>hyaluronic acid-QD</u> construct traces real time in vivo lymphatic vessel formation in mouse ear tissues. <sup>68</sup> The QD surface was stabilized with positively charged N-(2-aminoethyl)-6,8-dimercaptooctanamide (amine-DHLA) followed by electrostatic binding of QD-amine-DHLA with anionic HA in 1:1 to 4:1 ratios (Figure 16). The QD-amine-DHLA/hyaluronic acid construct specifically targets

overpopulated LYVE-1 on lymphatic vessels without major cytotoxicity. When injected subcutaneously into the ears of nude mice, the QD/ hyaluronic acid (4:1) probe reveals lymphatic vessel formation. <sup>68</sup>

#### Sea-urchin sperm

<u>N-acetylglucosamine (GlcNAc)</u> modified quantum dots (GlcNAc-QD) probe the localization of the GlcNAc binding proteins on the cell surface of a sperm. (Figure 17, A and B). Confocal images show the aggregation of GlcNAc-QDs on seaurchin sperm heads while mannose-QDs label the sperm body. <sup>69</sup>

## **Therapeutics**

Multivalent displays of ligands regulate physiological events by switching on or off cell's signal transduction. Metal nanoparticles (NPs) provide a platform for multiple ligand attachment and display. Glycan decorated NPs (GNPs) can cluster cell membrane receptors, stimulate intracellular signaling cascade,

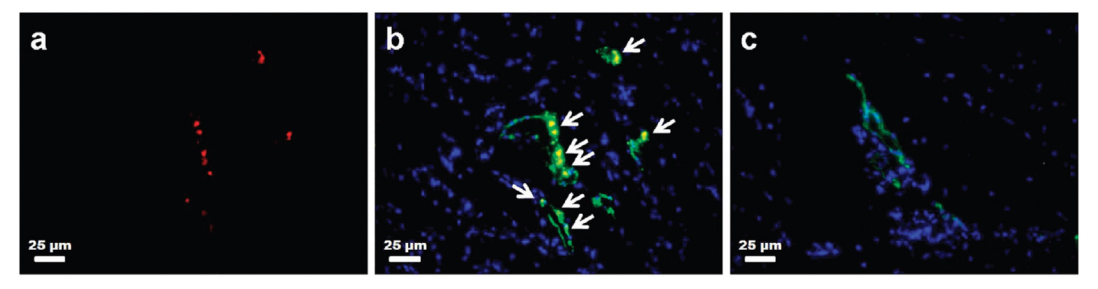


Figure 16. "Fluorescence microscope images of mouse ear tissues near the hyaluronic acid-quantum dot conjugate (HA-QD) injection site (**A**, **B**) and near the unconjugated QD injection site (**C**). The mouse ear tissues are vertically sectioned at 30 min after the subcutaneous injection of 200 nM HA-QD or unconjugated QD solution. The tissues are stained simultaneously by DAPI and fluorescent LYVE-1 antibodies. (**A**) Filter set is chosen to selectively show red fluorescence from QDs. (**B**, **C**) Fluorescence images are merged to overlay the red (QD), green (LYVE-1), and blue (DAPI) signals. The bright yellow co-localization spots of QD and LYVE-1 signals are indicated by arrow-heads in (**B**)." With permission from Bhang SH, Won N, Lee T-J, et al. Hyaluronic acid-quantum dot conjugates for in vivo lymphatic vessel imaging. *ACS Nano*. 3(6), 1389–1398 (2009), copyright American Chemical Society, Washington DC, 2009.

and correct "rogue" signaling pathways. <sup>70,71</sup> Alternatively, such multivalent GNPs might spatially sequester such pathways and remedy insult on physiological health. <sup>71</sup>

Novel GNPs were also synthesized to mimic viral particles and block viral entry, intracellular replication, and budding from the host cells. <sup>72</sup> In this section, we will discuss the therapeutic applications of GNPs.

#### Anti-cancer therapy

Metastasizing cancer cells take advantage of "sticky" glycans on the cancer cell to latch onto the endothelial cell surface, away from the primary site of cancer. <sup>73</sup> GNPs interfere with the cancer cell–endothelial cell interaction and reduce the stickiness of cancer cells through multivalent glycan presentation.

#### Anti-adhesive treatment

Adhesiveness of cancer cells with vascular endothelium is one of the hallmarks of cancer metastasis. Abnormal glycans on cancer cell surfaces interact with glycosphingolipids (GPLs) on the endothelial cell surface and mediate the adhesion. Murine melanoma cells express ganglioside GM3 (NeuNAc2 $\alpha$ 3Gal $\beta$ 4Glc $\beta$ Cer), which binds with lung endothelium GPLs—lactosylceramide (Gal $\beta$ 4Gal $\beta$ 4Cer), Gg3 (GalNAc $\beta$ 4Gal $\beta$ 4Glc $\beta$ Cer), and Gb4 (GalNAc $\beta$ 3Gal $\alpha$ 4-Gal $\beta$ 4Glc $\beta$ Cer). Thus, Rojo et al hypothesized that GNPs could interfere with the carbohydrate—carbohydrate interactions and disrupt the adhesion. They synthesized Au NPs displaying cluster-lactosides (70 lactose molecules) along with control GNPs (maltose-Au and glucose-Au) to test this hypothesis (Figure 18).

The efficacy of cluster-lacto-Au as an anti-adhesive agent was evaluated in C57/BI6 mice inoculated with B16F10 melanoma cells that metastasized at the lungs. The B16F10 cells incubated with cluster-lacto-Au NPs protected the lungs from metastasis. The efficacy of the cluster-lacto-AuNPs was confirmed through a fluorescent imaging experiment. Cluster-lacto-AuNPs incubated with dye-labeled B16F10 cells reduced endothelial cell adhesion. This demonstrated the therapeutic role of GNPs in treating advanced stage cancer and potential for clinical trials in the future.

## Heparan sulfate tetrasaccharides in cancer therapeutics

Jain et al synthesized a library of heparan sulfate tetrasaccharides to study their affinity for the epidermal growth factor (EGF) and heparin-binding EGF-like growth factors (HB-EGFs) (HB-EGF)—ligands for EGF receptors (EGFRs) and clinical targets for anticancer drug discovery. Among HS oligosaccharides with various O-sulfate codes, only 6-O-sulfate HS tetrasaccharide inhibited HB-EGF binding to native HS at IC $_{50}=126.6~\mu M$ . Surface plasmon resonance (SPR) studies determined the dissociation constant (K $_{D}$ ) = 11.12  $\mu M$ . When 6-O-phosphate HS tetrasaccharide was used against HB-EGF, the ELISA and SPR studies furnished IC $_{50}=97.13~\mu M$  and (K $_{D}$ ) = 11.06  $\mu M$ . Thus, the sulfated and phosphated HS tetrasaccharides can mediate the activation of EGFRs via HS/HB-EGF/EGFR complex.

Next, the authors constructed gold-heparan sulfate tetrasaccharide-6-O-sulfate (Au-HS-6-O-S) and gold-heparan sulfate tetrasaccharide-6-O-phosphate (Au-HS-6-O-P) to target breast cancer cells. The MDA-MB-468 cell lines endocytosized Au-HS-6-O-S at ~70-80% in 4 h, but showed hardly any response towards Au-HS-6-O-P. The Au-HS-6-O-S also selectively targeted the MDA-MB-468 cells in fibroblast cell cocultures. This study suggests the critical role of 6-O-sulfate HS tetrasaccharide in activating EGFRs and their anti-cancer therapeutic potentials.

## Infectious diseases

Viral infection is triggered by the interaction between viral envelop glycoproteins with host cell surface receptors which mainly consist of glycoconjugates. Thus, host cell surface glycans play a pivotal role in viral entry and its subsequent intracellular replication. GNPs can imitate viral particles (or host cells), interfere with the virus—cell membrane interactions, and protect the host cells from infections.

#### Herpes simplex virus-1 (HSV-1)

HSV-1 infection causes cold sores of the mouth and lips. The virus is approximately 170-200 nm in diameter with an icosahedral capsid encompassing DNA material and glycoproteins on the lipid bilayer. Positively charged residues of the glycoprotein C (gC) bind negatively charged glycosaminoglycans (GAGs), heparan sulfate (HS), or chondroitin sulfate (CS) on host cell membranes. This electrostatic interaction facilitates high-affinity viral attachment and its subsequent entry.

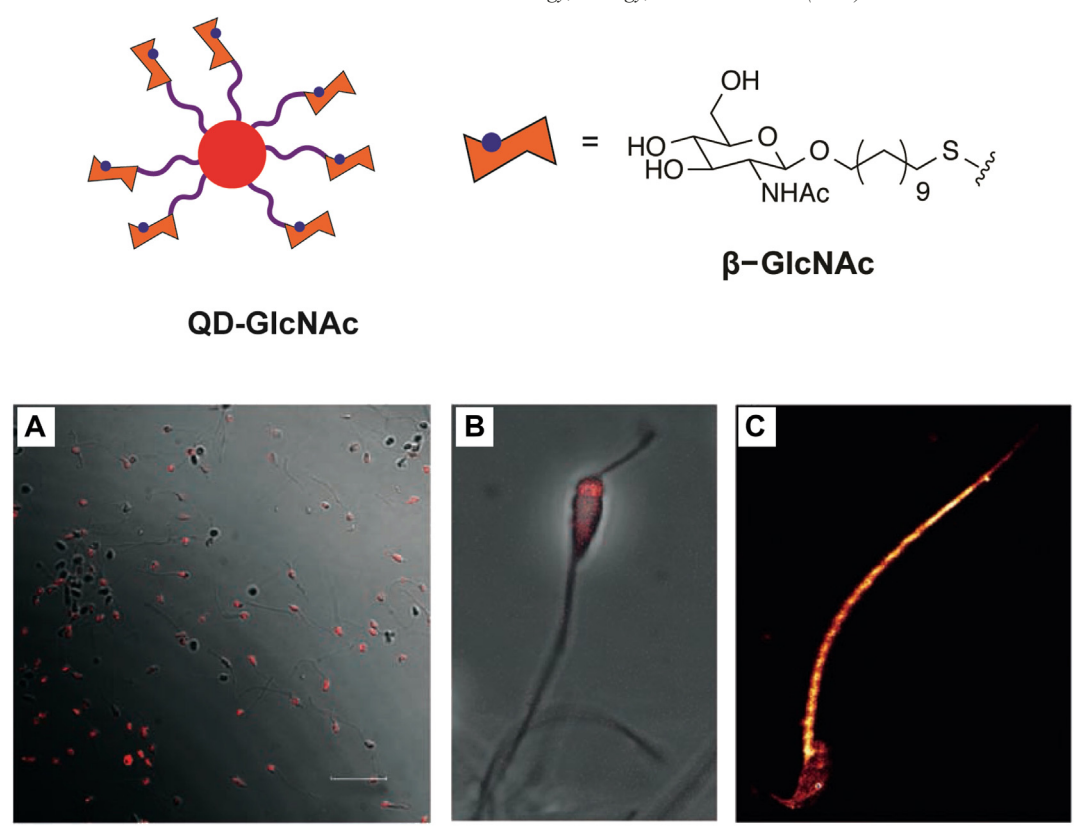


Figure 17. (A) *N*-acetylglucosamine (GlcNAc) labeled quantum dots (GlcNAc-QD) detect the localization of the GlcNAc binding proteins on the cell surface of a sperm. (B) "Confocal microscope imaging for staining of sperm with glycoquantum dots: (A) selective QDGLN labeling on the heads of sea-urchin sperm (scale bar = 20 mm), (B) close-up of QDGLN-labeled sea-urchin sperm, and C) close-up of QDMAN-labeled mouse sperm." With permission of Robinson A, Fang J-M, Chou P-T, Liao K-W, Chu R-M, Lee S-J. Probing lectin and sperm with carbohydrate-modified quantum dots. *Chembiochem.* 6(10), 1899–1905 (2005), copyright Wiley & Sons, Hoboken, NJ.

The HSV-1 infection can be reduced and potentially inhibited by a GAG mimic, which competes for the binding sites on the virus. Mercaptoethanesulfonate (MES) decorated gold (Au) or silver (Ag) nanoparticles imitated the sulfation density and multivalency of GAGs. The nano-construct interfered with virus attachment and entry into the cell and inhibited HSV-1 infection. Cell-to-cell infection was also contained and restricted to a small population. The nano-construct most likely achieved this feat by entering into intercellular space and interfering with viral fusion events. MES-Au or MES-Ag particles, the GAG mimic, provide docking sites for various viruses and thereby block the spread of viral infection.

## Human immunodeficiency virus (HIV-1)

HIV is a retrovirus with gp120 and gp41 glycoprotein envelopes. The high affinity binding of gp120 with CD4 (a receptor present on T-cells, macrophages, dendritic cells, and microglial cells) drives the HIV infection cascade. <sup>78</sup> Heavily N-glycosylated gp120/41 evades the host immune cells by concealing immunogenic peptides on the virus. The gp120 also targets C-type lectin dendritic cell-specific intracellular adhesion molecule-3-grabbing non-integrin (DC-SIGN) on dendritic cells. This strategy of dodging the host cell's immune surveillance through heavy mannose clusters on HIV-1 inspired Martínez-Avila et al to construct mannose decorated Au-NPs. <sup>19</sup> These

GNPs mimicked HIV-1 particles, disrupted gp120/41 interactions with immune cells, and wielded therapeutic potential.

A library of cluster mannoside-Au NPs is synthesized by using various *manno*- oligosaccharides with various thiol (-SH) capped spacers that impart hydrophilicity and/or hydrophobicity to the GNPs. The conjugation between *manno*-oligosaccharide and Au was a two-step procedure. First step involved direct glycosylation of mannose with either thiol- or amine-terminated linker, which was further modified to an amide bond and thiourea functionality. The thiourea linkage imparted versatility and efficiency in product yields. Second step immobilized various concentrations of cluster mannose on Au to afford multivalent *manno*- displaying GNPs (Figure 19).

The competitive inhibition of DC-SIGN/gp120 binding observed through surface plasmon resonance (SPR) demonstrated the terminal  $manno-\alpha 1-2manno-\alpha$  linkage (either free or conjugated with Au) is crucial for binding DC-SIGN receptor and inhibiting gp120 interaction. <sup>19</sup> Table 3 details the inhibitory effect of different GNPs towards gp120. The inhibitory potencies of GNPs remained unchanged as the complexity of cluster mannosides increased.

## Anti-bacterial treatment

Several Gram-negative bacteria such as *Escherichia coli* O157: H7 and *Shigella dysetriae* release Shiga toxins (Stx), a member of

#### **Anti-Adhesive Treatment**

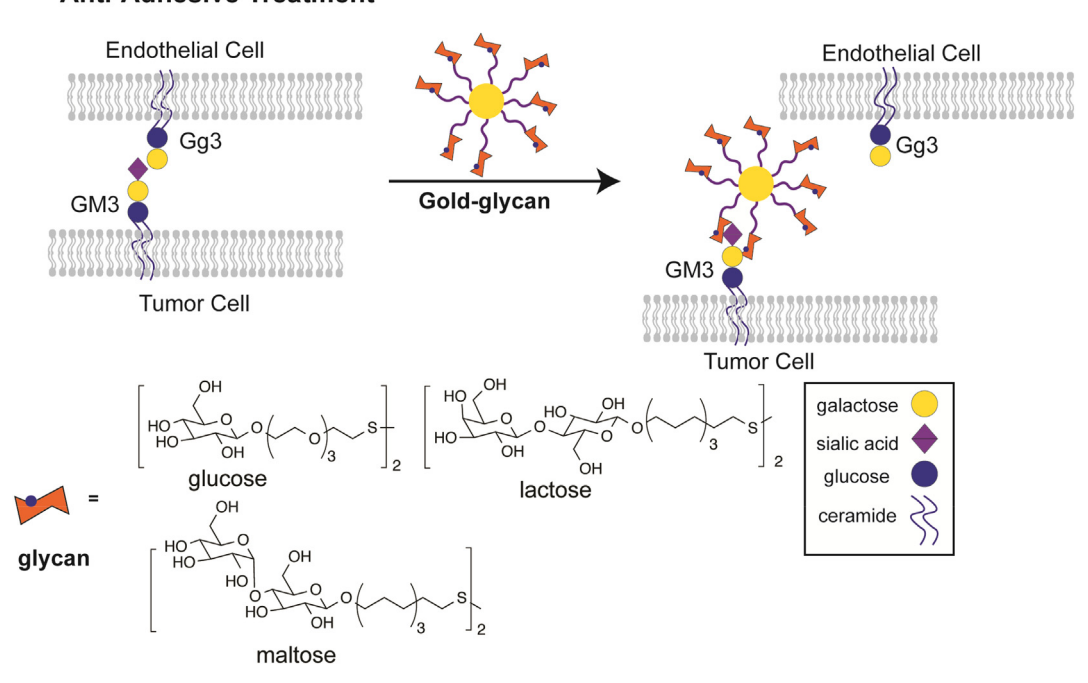


Figure 18. Glycosynapse disruption. Gold-lactose glyco-nanoparticle binds the GM3 glycosphingolipid on a cancer cell surface, sequesters the Gg3 lacto-sylceramide receptor on endothelial cells, and prevents adhesion and spreading of the cancer cells.

AB<sub>5</sub> toxins family. <sup>79</sup> Domain A drives RNA N-glycosidase catalytic activity and domain B binds glycolipids, lipid raft like structures present on host cell surfaces. The domain B binds globotriaosylceramide (Gb3) glycolipid consisting of Pk trisaccharide (Pk-trisacch), delivers domain A to the cytoplasmic region of the host cell, and propels the cascade of infection. Stx is implicated in hemolytic uremic syndrome (HUS), kidney, and neurological disorders. The Stx antigens (Stx1 and Stx2) recognize Pk trisaccharide fine structures. These subtly distinct interactions translate into varied toxin potency.

Kulkarni et al synthesized competitive inhibitors of Stx by immobilizing two copies of thiolated Pk-trisacch and galactose on AuNPs <sup>80</sup> (Figure 20). Only an N-acetyl (-NHCOCH<sub>3</sub> or NAc) group at the 2-position of central galactose moiety distinguished these two trisaccharides. The NAc-Pk-trisacch occupied on GNP2 supplied strong interaction energy and neutralized Stx2 only. However, the Pk-trisacch-GNP1 selectively nullified Stx1. The galactose only GNP3 failed to neutralize the Stx. When two variants of Stx2 (Stx2c and Stx2d) were tested against the GNPs, their neutralizing potency was profoundly impacted by a subtle difference in the amino acid sequence of the two variants.

#### Vaccines

Decorating GNPs with glycan antigens expressed on cancer cells produces anti-cancer vaccines. In this section, we discuss two seminal reports.

#### Anticancer vaccines

Anticancer vaccines target tumor associated carbohydrate antigens (TACAs). 81,82 Oligosaccharides covalently linked with carrier proteins perform as immunogen and mobilize immune

response. These tumor-associated glycopeptides stimulate T helper cells and propel the cascade of antibody production. The clustering of disaccharides and/or oligosaccharides might drive this immunity. For example, glyco-clustering appears to play a vital role in antibody recognition of disaccharide antigens such as silyl-Tn (sTn) and a tetrasaccharide antigen, Lewis<sup>y</sup>. The sTn epitope enriches the endothelial cancer cells, while Lewis<sup>y</sup> performs as an antigen associated with colon, liver, prostate, and ovarian carcinomas.

GNPs furnish the platform for multivalent presentation of the TACAs. This might increase the antibody density, eliciting multiple antibody responses to target different cancer types. Gold nanoparticles decorated with sTn and Lewis<sup>y</sup> antigens, a Thelper peptide from tetanus toxoid (TT), and glucose were constructed to develop GNP-based anticancer vaccines. <sup>83</sup> These ligands were conjugated with thiol-capped linkers for Au stabilization. A library of 10 vaccine candidates was synthesized with varying ligand ratios and densities (Figure 21). From this work, the GNPs were found to elicit a weak immune response in mice.

In another study, Au NPs were immobilized with TACAs, C3d peptide (28 -mer) for B-cell activation, and a nonfunctional linker. <sup>18</sup> Pancreatic adenocarcinoma cell surface mucin, MUC4, decorated with Thomsen Friedenreich (TF) antigen, performed as TACA. A library of six glycopeptides was prepared through solid-state synthesis for AuNP conjugation. The evaluation of sera from the GNP immunized mice showed small but statistically significant production of IgM and IgG antibodies.

## Anti-pneumococcal vaccine

The capsular polysaccharide (CPS) of *Staphylococcus pneu-moniae* determines the pathogenicity. The CPS consists of tri-

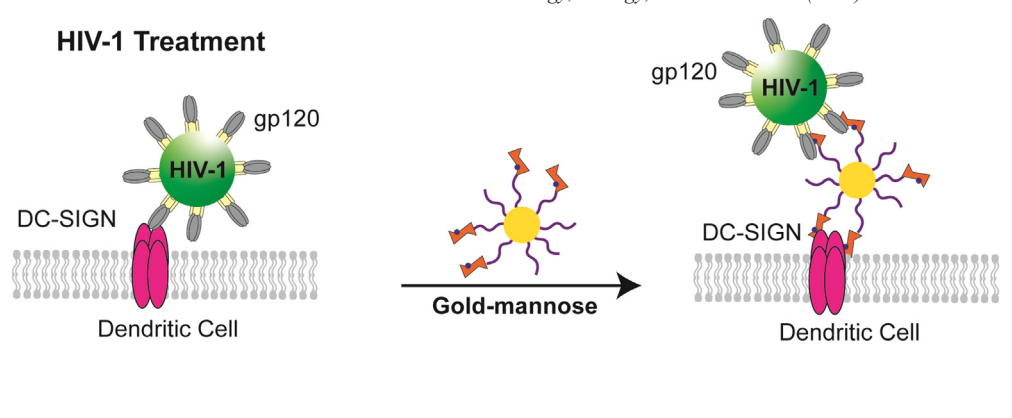


Figure 19. The gp120 glycoprotein on HIV-1 envelope binds high-mannose DC-SIGN receptor on dendritic cell and mediates viral entry. A glyco-nanoparticle mimetic consisting of mannoses (varied concentrations) arrests this interaction, isolates gp120 from DC-SIGN receptor, and inhibits the viral entry.

Table 3
Inhibition of DC-SIGN binding with gp120 through *Manno-*GNPs. 19

| GNP | Mannose linkage    | Average number of mannose/GNP | [C <sub>100</sub> ]/GNP (μM) | [C <sub>100</sub> ]/mannose (μM) |
|-----|--------------------|-------------------------------|------------------------------|----------------------------------|
|     | Manα1-2Manα        | 25                            | 0.115                        | 2.9                              |
|     | Manα1-3Manα        | 19                            | 4.3                          | 82                               |
|     | Manα1-2Manα1-2Manα | 25                            | 1.2                          | 30                               |
|     | Manα1-2Manα        | 59                            | 0.08                         | 4.7                              |
|     | Manα1-2Manα        | 22                            | 0.13                         | 2.9                              |

[C<sub>100</sub>] is the concentration of GNPs required to inhibit gp120 binding with DC-SIGN.

19F, trisaccharide fragment of serotype 19F, and tetra-14, tetrasaccharide fragment of serotype 14. Gold nanoparticles occupied with these two antigens, glucose (for biocompatibility), and ovalbumin peptide 323-339 (OVAp) might vaccinate against *S. pneumoniae* (Figure 22). <sup>84</sup> The OVAp targets OVA-specific T helper cell receptors and mobilizes the immune system.

Differential ratios of the ligands produced differential GNP vaccines: GNP-1 (Tri-19F/Tetra-14/Glc/OVAp = 40:40:15:5), GNP-2 (Tri-19F/Glc/OVAp = 45:50:5), GNP-3 (Tri-19F/OVAp = 95:5), and GNP-4 (Tetra-14/Glc/OVAp = 45:50:5). The GNP-1 vaccine generated IgG antibodies (IgG-1, IgG-2a and IgG2b subclasses) against tetra-14, but reported no IgG antibody against tri-19F antigen. This study predicts GNPs as potential vaccine candidates against infection.

#### Anti-tuberculosis vaccine

In an attempt to develop a vaccine against mycobacterial infections, Burygin et al designed gold nanoparticle conjugated hexaarabinofuranoside — an integral component of lipoarabinomannan (LAM) and arabinogalactan (AG) of the bacterial cell wall. <sup>85</sup> The authors deployed two gold-hexaarabinofurano-

side constructs with varying spacer length: short and hydrophobic  $C_2$  ( $-CH_2CH_2-$ ) and long and hydrophilic  $C_2EG_7$  ( $-CH_2CH_2-$ NHCOCH<sub>2</sub>-(OCH<sub>2</sub>CH<sub>2</sub>)<sub>6</sub>–). Both nanoparticles induced immune response in rabbits and produced antisera with polyclonal antibodies, equally effective in identifying LAM and AG oligosaccharide epitopes (limit of detection for hexaarabinofuranoside = 60 ng). ELISA tests demonstrated comparable performance of the two nanoparticles: strong interaction between the anti-sera with mycobacterial cells ( $M.\ bovis$ , and  $M.\ smegmatis$ ), weak interaction with  $M.\ phlei$ , and no interaction with  $E.\ coli.$ 

This study clearly shows the promise of glyconanotechnology in the development of *M. tuberculosis* vaccine to end the TB epidemic by 2030, in line with the End TB strategy of the World Health Organization (WHO).

## Challenges and outlook

We have highlighted promises of GNPs in developing diagnostic, therapeutic, and analytical strategies. In spite of significant progress, nanotechnology solutions need to address the

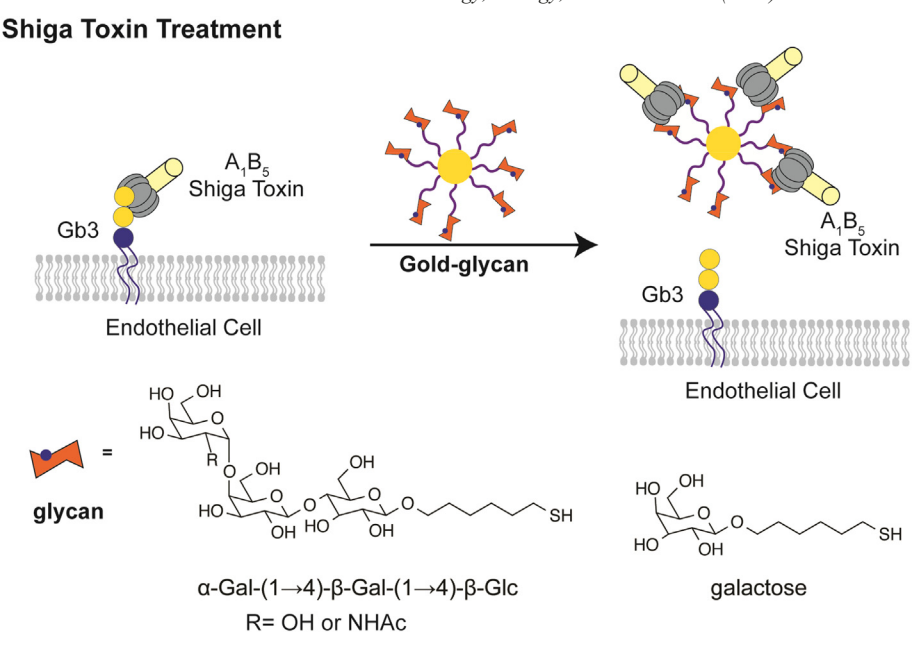


Figure 20. The B-subunit pentamer of Shiga toxin released by *E. coli*, *S. dysentriae* pathogens binds to Gb3 glycosphigolipid on an endothelial cell. Gold-trisaccharide nanoparticle mimics the Gb3 epitope and neutralizes the B-subunit. The glyco-nanoparticle inhibits internalization and cytosolic translocation of the Shiga toxin.

metal cytotoxicity, slow rate of reporting and clearance from the disease site, and lack of convenient synthetic procedure for complex carbohydrates. Glycan conjugation enhances the biocompatibility of the otherwise toxic metal nanoparticles, but slow targeting, reporting (diagnosis), and clearance through the body's disposal system complicate such compatibility. Ref. 86,87 Vigorous investment in research and development shall transform GNP research, produce novel 'smart' materials, and translate GNPs from bench to bedside. The discovery of chemoenzymatic and solid-phase automated synthesis of complex carbohydrates has opened windows of opportunities to study the functions of complex carbohydrate conjugated nanomaterials.

NHLBI's carbohydrate training program, through the program of excellence in glycosciences (PEG), trained a new generation of scientists to tackle biomedical problems. The goal of this program was to place glycoscience in the middle of mainstream biology, create a sustainable workforce that can solve biological problems from a glycoscience standpoint, and integrate glycoscience in the medical and graduate school curricula. 89 This program encouraged confluence of all major chemical and biomedical disciplines with glycoscience. Such initiative can potentially revolutionize glyco-nanotechnology. Knowledge gained from such programs will aid development of novel 'smart' GNPs that can improve disease diagnosis, treatment (and/or theranostic), drug delivery (nanorobots), mimic 'glycocalix' of various microbes (vaccine) and eukaryotic cells, modulate the innate and adaptive immune system, and perform as multimodal imaging probes (for example, MRI/PET, MRI/fluorescent). 90 We will also need the FDA for successful translation of glyco-nanotechnology. The FDA's 2020 nanotechnology report highlighted its effort to develop standards through stakeholder involvement, monitor convergence of emerging technologies with nanomaterials, and support innovative nanotechnology products. Such efforts will converge

academics, investors from industry and the government, and contract research and manufacturing organizations. 91

Finally, scaling up nanomaterial production from milligrams to the kilogram scale faces three immediate obstacles: change in the functional properties, inconsistent performance of each synthetic batch, and thus lack of industry interest in commercialization. <sup>92</sup>

In 2010, the United States Department of Energy created the Materials Engineering Research Facility (MERF) at the Argonne National Laboratories to address the problems of scalability. <sup>93</sup> The US government mandated MERF to generate reliable large-scale manufacturing of nanomaterials with consistent performance at low cost. If successful, MERF will provide a technology transfer package detailing the process to a potential industry partner. In 2011, the National Science Foundation (NSF) started Scalable Nanomanufacturing (SNM) Solicitation to build manufacturing technologies for future economic possibilities. 94,95,96 The new economic engine will involve basic research in scalable nanopatterning, their integration into electronic and optoelectronic devices, and in some cases, non-electronic instruments, and generate high value end products that benefit society and economy. Scaling up nanopatterning of large area surfaces encompasses printing, lithography and self-assembly, and 3D nanofabrication. When the scalability problem is addressed successfully, a new nanomanufactured economy will finally arrive.

## Conclusion

In this review, we underscored the emerging glyconanotechnology through multiple examples that might inspire novel 'smart' materials. The GNPs display multiple copies of glycans that target aberrant ECM, report this aberration through optical, magnetic, and electric signals, and identify pathology.

#### **Anticancer Vaccine**

Figure 21. Anticancer glyco-nano vaccines. (A) Tetanus toxoid (TT) peptide-gold-silyl-Tn/Le Y glyco-nanoparticle presents two cancer antigens: sialyl-Tn, a mucin-associated antigen expressed on epithelial cancer and Le Y antigen for colon, liver, and prostate cancer. (B) C3d-peptide-gold-glycan vaccine exploits glycopeptides (consisting of Thomsen–Friedenreich (TF) disaccharide) of pancreatic adenocarcinoma and C3d adjuvant to elicit IgG and IgM antibody production.

Glyconanotechnology was engaged to determine life-threatening contaminants in the pharmaceutical-grade heparin (gold-heparindye), glyco-fingerprint various tumors via MRI (iron oxideglycans), and map atherosclerosis (iron oxide-hyaluronic acid). The GNPs were also engineered to remedy 'rogue' signaling transduction in diseased cells. We discussed the therapeutic power of the glyconanoparticles — gold-lactose disrupts the glycosynapse between cancer and endothelial cells, goldmannoside outcompetes HIV-1 viruses, and gold decorated with tri-19F and tetra-14 induces immunological response against Staphylococcus pneumoniae. We highlighted the glyconanoparticles as robust analytical tools. For example, the paperbased lateral flow detection (FLD) system involving sialic acid conjugated gold nanoparticles detected the spike glycoprotein of the SARS-COV-1 in half an hour. In a subsequent study, the researchers developed a low-cost flow-through device that can detect SARS-COV-2 from nasal swabs. This device can solve the COVID testing problems, especially in the low income countries. During a raging pandemic, glyco-nanotechnology can solve

biomedical questions and improve public health. <sup>97</sup> Future materials will also involve glycans synthesized *via* enzymatic and chemo-enzymatic methods, custom-synthesized nanoparticles with defined structure—function, and development of multifunctional nanoparticles. <sup>98,99</sup> The initiatives by NHLBI and FDA will inspire innovative and cost-effective nanotechnologies that will likely benefit the patient.

#### **Credit Author Statement**

All three authors have written parts of the review. Mausam Kalita has prepared the figures. Macy Payne is responsible for combining all three parts into one review. Stefan Bossmann is responsible for the final revised version that is submitted here and for some adjustments of the figures.

## Acknowledgments

NSF 2129617.

# 

Figure 22. Anti-pneumococcal vaccine. Gold nanoparticles decorated with tri-19F (trisaccharide fragment of serotype 19F), tetra-14 (tetrasaccharide fragment of serotype 14), and OVAp (T helper peptide) stimulate the immune system to generate IgG antibodies against tetra-14, while no IgG antibody was reported against tri-19F antigen.

(T helper peptide)

#### References

- Kelly KL, Coronado E, Zhao LL, Schatz GC. The optical properties of metal nanoparticles: the influence of size, shape, and dielectric environment. J Phys Chem B 2003;107(3):668-77.
- Thakor AS, Jokerst JV, Ghanouni P, Campbell JL, Mittra E, Gambhir SS. Clinically approved nanoparticle imaging agents. *J Nucl Med* 2016; 57(12):1833-7.
- Ventola CL. Progress in nanomedicine: approved and investigational nanodrugs. P T 2017;42(12):742-55.
- Bobo D, Robinson KJ, Islam J, Thurecht KJ, Corrie SR. Nanoparticlebased medicines: a review of FDA-approved materials and clinical trials to date. *Pharm Res* 2016;33(10):2373-87.
- Abo-Zeid Y, Ismail NSM, McLean GR, Hamdy NM. A molecular docking study repurposes FDA approved iron oxide nanoparticles to treat and control COVID-19 infection. *Eur J Pharm Sci* 2020; 153105465.
- Muthana SM, Campbell CT, Gildersleeve JC. Modifications of glycans: biological significance and therapeutic opportunities. ACS Chem Biol 2012;7(1):31-43.
- Parker RB, Kohler JJ. Regulation of intracellular signaling by extracellular glycan remodeling. ACS Chem Biol 2010;5(1):35-46.
- Ohtsubo K, Marth JD. Glycosylation in cellular mechanisms of health and disease. Cell 2006;126(5):855-67.
- Marth JD, Grewal PK. Mammalian glycosylation in immunity. Nat Rev Immunol 2008;8(11):874-87.
- Rabinovich GA, Croci DO. Regulatory circuits mediated by lectin-glycan interactions in autoimmunity and cancer. *Immunity* 2012;36(3): 322-35
- 11. Chen X, Ramström O, Yan M. Glyconanomaterials: emerging applications in biomedical research. *Nano Res* 2014;7(10):1381-403.

- Reichardt NC, Martín-Lomas M, Penadés S. Glyconanotechnology. Chem Soc Rev 2013;42(10):4358-76.
- Weingart JJ, Sun X-L. Glyco-functionalized quantum dots. In: Huang X, Barchi JJ, editors. *Petite and Sweet: Glyco-nanotechnology as a bridge* to new medicines. Washington, DC: American Chemical Society; 2011. p. 105-21.
- van Kasteren SI, Campbell SJ, Serres S, Anthony DC, Sibson NR, Davis BG. Glyconanoparticles allow pre-symptomatic in vivo imaging of brain disease. *Proc Natl Acad Sci U S A* 2009;106(1):18-23.
- Lee H, Lee K, Kim IK, Park TG. Synthesis, characterization, and in vivo diagnostic applications of hyaluronic acid immobilized gold nanoprobes. *Biomaterials* 2008;29(35):4709-18.
- Kim KS, Hur W, Park S-J, et al. Bioimaging for targeted delivery of hyaluronic acid derivatives to the livers in cirrhotic mice using quantum dots. ACS Nano 2010;4(6):3005-14.
- Rojo J, Díaz V, de la Fuente JM, et al. Gold glyconanoparticles as new tools in antiadhesive therapy. *Chembiochem* 2004;5(3):291-7.
- Brinas RP, Sundgren A, Sahoo P, et al. Design and synthesis of multifunctional gold nanoparticles bearing tumor-associated glycopeptide antigens as potential cancer vaccines. *Bioconjug Chem* 2012;23(8):1513-23.
- Martínez-Avila O, Hijazi K, Marradi M, et al. Gold manno-glyconanoparticles: multivalent systems to block HIV-1 gp120 binding to the lectin DC-SIGN. *Chem Eur J* 2009;15(38):9874-88.
- He X-P, Hu X-L, Jin H-Y, et al. Quick serological detection of a cancer biomarker with an agglutinated supramolecular glycoprobe. *Anal Chem* 2015;87(17):9078-83.
- Dai Z, Kawde A-N, Xiang Y, et al. Nanoparticle-based sensing of glycan-lectin interactions. J Am Chem Soc 2006;128(31):10018-9.
- Wang X, Matei E, Deng L, Ramström O, Gronenborn AM, Yan M. Multivalent glyconanoparticles with enhanced affinity to the anti-viral lectin Cyanovirin-N. *Chem Commun* 2011;47(30):8620-2.

- Kalita M, Balivada S, Swarup VP, et al. A nanosensor for ultrasensitive detection of oversulfated chondroitin sulfate contaminant in heparin. J Am Chem Soc 2014;136(2):554-7.
- Tateno H, Nakamura-Tsuruta S, Hirabayashi J. Comparative analysis of core-fucose-binding lectins from Lens culinaris and Pisum sativum using frontal affinity chromatography. Glycobiology 2009;19(5):527-36.
- Okamatsu M, Feng F, Ohyanagi T, et al. Fluorescence polarizationbased assay using N-glycan-conjugated quantum dots for screening in hemagglutinin blockers for influenza A viruses. *J Virol Methods* 2013; 187(2):390-4.
- Dandliker WB, Kelly RJ, Dandliker J, Farquahar J, Levin J. Fluorescence polarization immunoassay. Theory and experimental method. *Immunochemistry* 1973;10(4):219-27.
- Jameson DM, Ross JA. Fluorescence polarization/anisotropy in diagnostics and imaging. Chem Rev 2010;110(5):2685-708.
- Ding L, Cheng W, Wang X, Ding S, Ju H. Carbohydrate monolayer strategy for electrochemical assay of cell surface carbohydrate. *J Am Chem Soc* 2008;130(23):7224-5.
- Schofield CL, Field RA, Russell DA. Glyconanoparticles for the colorimetric detection of cholera toxin. Anal Chem 2007;79(4):1356-61.
- Jeong H-H, Kim Y-G, Jang S-C, Yi H, Lee C-S. Profiling surface glycans on live cells and tissues using quantum dot-lectin nanoconjugates. *Lab Chip* 2012;12(18):3290-5.
- Malik A, Lee J, Lee J. Community-based network study of proteincarbohydrate interactions in plant lectins using glycan array data. *PLoS One* 2014:9(4)e95480.
- Wearne KA, Winter HC, O'Shea K, Goldstein IJ. Use of lectins for probing differentiated human embryonic stem cells for carbohydrates. *Glycobiology* 2006;16(10):981-90.
- Gupta B, Sadaria D, Warrier VU, et al. Plant lectins and their usage in preparing targeted nanovaccines for cancer immunotherapy. Semin Cancer Biol 2022;80:87-106.
- Müller S, Hanisch F-G. Recombinant MUC1 probe authentically reflects cell-specific O-glycosylation profiles of endogenous breast cancer mucin. High density and prevalent core 2-based glycosylation. *J Biol Chem* 2002;277(29):26103-12.
- Wang X, Matei E, Deng L, Ramström O, Gronenborn AM, Yan M. Multivalent glyconanoparticles with enhanced affinity to the anti-viral lectin Cyanovirin-N. *Chem Commun* 2011;47(30):8620-2.
- Cheng HC. The power issue: determination of KB or Ki from IC50. A closer look at the Cheng-Prusoff equation, the Schild plot and related power equations. J Pharmacol Toxicol Methods 2001;46(2):61-71.
- Nolting B, Yu J-J, Liu G, Cho S-J, Kauzlarich S, Gervay-Hague J. Synthesis of gold glyconanoparticles and biological evaluation of recombinant gp120 interactions †. *Langmuir* 2003;19(16):6465-73.
- Baker AN, Richards S-J, Guy CS, et al. The SARS-COV-2 spike protein binds sialic acids and enables rapid detection in a lateral flow point of care diagnostic device. ACS Cent Sci 2020;6(11):2046-52.
- Baker AN, Richards S-J, Pandey S, et al. Glycan-based flow-through device for the detection of SARS-COV-2. ACS Sens 2021;6(10): 3696-705.
- Kalita M, Chua JS, Boothello RS, et al. Visualizing antithrombinbinding 3-O-sulfated heparan sulfate motifs on cell surfaces. *Chem Commun* 2020;56(92):14423-6.
- Thacker BE, Xu D, Lawrence R, Esko JD. Heparan sulfate 3-O-sulfation: a rare modification in search of a function. *Matrix Biol* 2014;35: 60-72.
- Zhao J, Zhu Y, Song X, et al. 3-O-Sulfation of heparan sulfate enhances tau interaction and cellular uptake. *Angew Chem Int Ed Eng* 2020;**59**(5): 1818-27
- Chuang Y-J, Zhou X, Pan Z, Turchi C. A convenient method for synthesis of glyconanoparticles for colorimetric measuring carbohydrate-protein interactions. *Biochem Biophys Res Commun* 2009;389(1):22-7.
- 44. Kikkeri R, Padler-Karavani V, Diaz S, et al. Quantum dot nanometal surface energy transfer based biosensing of sialic acid compositions and linkages in biological samples. *Anal Chem* 2013;85(8):3864-70.

- Triulzi RC, Micic M, Giordani S, Serry M, Chiou W-A, Leblanc RM. Immunoasssay based on the antibody-conjugated PAMAM-dendrimergold quantum dot complex. *Chem Commun* 2006;48:5068-70.
- 46. Griffin J, Singh AK, Senapati D, et al. Size- and distance-dependent nanoparticle surface-energy transfer (NSET) method for selective sensing of hepatitis C virus RNA. Chem Eur J 2009;15(2):342-51.
- Poole J, Day CJ, von Itzstein M, Paton JC, Jennings MP. Glycointeractions in bacterial pathogenesis. *Nat Rev Microbiol* 2018;16(7):440-52.
- El-Boubbou K, Gruden C, Huang X. Magnetic glyco-nanoparticles: a unique tool for rapid pathogen detection, decontamination, and strain differentiation. J Am Chem Soc 2007;129(44):13392-3.
- Cipolla L, Gregori M, So P-W. Glycans in magnetic resonance imaging: determinants of relaxivity to smart agents, and potential applications in biomedicine. *Curr Med Chem* 2011;18(7):1002-18, https://doi.org/10. 2174/092986711794940851.
- Pan C, Lin J, Zheng J, Liu C, Yuan B, Akakuru OU, et al. An intelligent T1–T2 switchable MRI contrast agent for the non-invasive identification of vulnerable atherosclerotic plaques. *Nanoscale* 2021;13:6461-74, https://doi.org/10.1039/d0nr08039j.
- Läubli H, Borsig L. Selectins promote tumor metastasis. Semin Cancer Biol 2010;20(3):169-77.
- Kouyoumdjian H, Zhu DC, El-Dakdouki MH, et al. Glyconanoparticle aided detection of β-amyloid by magnetic resonance imaging and attenuation of βamyloid induced cytotoxicity. ACS Chem Neurosci 2013;4(4):575-84.
- El-Boubbou K, Zhu DC, Vasileiou C, et al. Magnetic glyco-nanoparticles: a tool to detect, differentiate, and unlock the glyco-codes of cancer via magnetic resonance imaging. *J Am Chem Soc* 2010;132(12):4490-9.
- Marradi M, Alcántara D, de la Fuente JM, García-Martín ML, Cerdán S, Penadés S. Paramagnetic Gd-based gold glyconanoparticles as probes for MRI: tuning relaxivities with sugars. *Chem Commun* 2009;26:3922-4.
- El-Dakdouki MH, El-Boubbou K, Kamat M, et al. CD44 targeting magnetic glyconanoparticles for atherosclerotic plaque imaging. *Pharm Res* 2014;31(6):1426-37.
- Zöller M. CD44: can a cancer-initiating cell profit from an abundantly expressed molecule? *Nat Rev Cancer* 2011;11(4):254-67.
- 57. Rios de la Rosa JM, Pingrajai P, Pelliccia M, et al. Binding and internalization in receptor-targeted carriers: the complex role of CD44 in the uptake of hyaluronic acid-based nanoparticles (siRNA delivery). Adv Healthc Mater 2019;8(24)e1901182.
- Lai C-H, Lin C-Y, Wu H-T, et al. Galactose encapsulated multifunctional nanoparticle for hepg2 cell internalization. *Adv Funct Mater* 2010; 20(22):3948-58.
- Roggenbuck D, Mytilinaiou MG, Lapin SV, Reinhold D, Conrad K. Asialoglycoprotein receptor (ASGPR): a peculiar target of liver-specific autoimmunity. *Auto Immun Highlights* 2012;3(3):119-25.
- Kamat M, El-Boubbou K, Zhu DC, et al. Hyaluronic acid immobilized magnetic nanoparticles for active targeting and imaging of macrophages. *Bioconjug Chem* 2010;21(11):2128-35.
- Lee K, Lee H, Bae KH, Park TG. Heparin immobilized gold nanoparticles for targeted detection and apoptotic death of metastatic cancer cells. *Biomaterials* 2010;31(25):6530-6.
- Desgrosellier JS, Cheresh DA. Integrins in cancer: biological implications and therapeutic opportunities. Nat Rev Cancer 2010;10(1):9-22.
- 63. Frigell J, García I, Gómez-Vallejo V, Llop J, Penadés S. 68Ga-labeled gold glyconanoparticles for exploring blood-brain barrier permeability: preparation, biodistribution studies, and improved brain uptake via neuropeptide conjugation. *J Am Chem Soc* 2014;136(1):449-57.
- Alivisatos AP. Semiconductor clusters, nanocrystals, and quantum dots. Science 1996;271(5251):933-7.
- Nirmal M, Brus L. Luminescence photophysics in semiconductor nanocrystals. Acc Chem Res 1999;32(5):407-14.
- Jackson DG, Prevo R, Clasper S, Banerji S. LYVE-1, the lymphatic system and tumor lymphangiogenesis. *Trends Immunol* 2001;22(6):317-21.
- Bono P, Wasenius V-M, Heikkilä P, Lundin J, Jackson DG, Joensuu H. High LYVE-1-positive lymphatic vessel numbers are associated with poor outcome in breast cancer. *Clin Cancer Res* 2004;10(21):7144-9.

- Bhang SH, Won N, Lee T-J, et al. Hyaluronic acid-quantum dot conjugates for in vivo lymphatic vessel imaging. ACS Nano 2009;3(6):1389-98.
- Robinson A, Fang J-M, Chou P-T, Liao K-W, Chu R-M, Lee S-J. Probing lectin and sperm with carbohydrate-modified quantum dots. Chembiochem 2005;6(10):1899-905.
- Jayaraman N. Multivalent ligand presentation as a central concept to study intricate carbohydrate-protein interactions. *Chem Soc Rev* 2009;38 (12):3463-83.
- Kiessling LL, Gestwicki JE, Strong LE. Synthetic multivalent ligands as probes of signal transduction. Angew Chem Int Ed Eng 2006;45(15): 2348-68
- García I, Marradi M, Penadés S. Glyconanoparticles: multifunctional nanomaterials for biomedical applications. *Nanomedicine (London)* 2010;5 (5):777-92.
- Häuselmann I, Borsig L. Altered tumor-cell glycosylation promotes metastasis. Front Oncol 2014:4:28.
- Kojima N, Hakomori S. Cell adhesion, spreading, and motility of GM3expressing cells based on glycolipid-glycolipid interaction. *J Biol Chem* 1991;266(26):17552-8.
- 75. Kojima N, Shiota M, Sadahira Y, Handa K, Hakomori S. Cell adhesion in a dynamic flow system as compared to static system. Glycosphingolipidglycosphingolipid interaction in the dynamic system predominates over lectin- or integrin-based mechanisms in adhesion of B16 melanoma cells to non-activated endothelial cells. J Biol Chem 1992;267(24):17264-70.
- Jain P, Shanthamurthy CD, Chaudhary PM, Kikkeri R. Rational designing of glyco-nanovehicles to target cellular heterogeneity. *Chem Sci* 2021;12(11): 4021-7.
- Baram-Pinto D, Shukla S, Gedanken A, Sarid R. Inhibition of HSV-1 attachment, entry, and cell-to-cell spread by functionalized multivalent gold nanoparticles. *Small* 2010;6(9):1044-50.
- Botos I, Wlodawer A. Proteins that bind high-mannose sugars of the HIV envelope. Prog Biophys Mol Biol 2005;88(2):233-82.
- Villysson A, Tontanahal A, Karpman D. Microvesicle involvement in Shiga toxin-associated infection. *Toxins (Basel)* 2017;9(11).
- Kulkarni AA, Fuller C, Korman H, Weiss AA, Iyer SS. Glycan encapsulated gold nanoparticles selectively inhibit Shiga toxins 1 and 2. Bioconjug Chem 2010;21(8):1486-93.
- Hakomori S. Tumor-associated carbohydrate antigens defining tumor malignancy: basis for development of anti-cancer vaccines. Adv Exp Med Biol 2001;491:369-402.
- Feng D, Shaikh AS, Wang F. Recent advance in tumor-associated carbohydrate antigens (TACAs)-based antitumor vaccines. ACS Chem Biol 2016;11(4):850-63.
- Ojeda R, de Paz JL, Barrientos AG, Martín-Lomas M, Penadés S. Preparation of multifunctional glyconanoparticles as a platform for po-

- tential carbohydrate-based anticancer vaccines. *Carbohydr Res* 2007; **342**(3–4):448-59.
- Vetro M, Safari D, Fallarini S, et al. Preparation and immunogenicity of gold glyco-nanoparticles as antipneumococcal vaccine model. *Nano-medicine (London)* 2017;12(1):13-23.
- Burygin GL, Abronina PI, Podvalnyy NM, Staroverov SA, Kononov LO, Dykman LA. Preparation and in vivo evaluation of glyco-gold nanoparticles carrying synthetic mycobacterial hexaarabinofuranoside. *Beilstein J Nanotechnol* 2020;11:480-93.
- Hockl PF, Wolosiuk A, Pérez-Sáez JM, et al. Glyco-nano-oncology: novel therapeutic opportunities by combining small and sweet. *Pharmacol Res* 2016;109:45-54.
- El-Boubbou K, Huang X. Glyco-nanomaterials: translating insights from the "sugar-code" to biomedical applications. *Curr Med Chem* 2011;18 (14):2060-78.
- Kuberan B, Beeler DL, Lech M, Wu ZL, Rosenberg RD. Chemoenzymatic synthesis of classical and non-classical anticoagulant heparan sulfate polysaccharides. *J Biol Chem* 2003;278(52): 52613-21.
- Agre P, Bertozzi C, Bissell M, et al. Training the next generation of biomedical investigators in glycosciences. J Clin Invest 2016;126(2): 405-8.
- Jokerst JV, Gambhir SS. Molecular imaging with theranostic nanoparticles. Acc Chem Res 2011;44(10):1050-60.
- https://www.fda.gov/science-research/nanotechnology-programs-fda/ nanotechnology-task-force 2020.
- 92. A matter of scale, editorial. Nat Nanotechnol 2016;11:733.
- 93. https://www.anl.gov/amd/materials-engineering-research-facility.
- 94. Cooper K. Scalable nanomanufacturing—a review. *Micromachines* (Basel) 2017;8(1):20.
- Scalable nanomanufacturing (SNM) solicitation Available online: http:// www.nsf.gov/pubs/2016/nsf16513/nsf16513.htm (accessed on 27 November 2016).
- NSI: Sustainable nanomanufacturing—creating the industries of the future Available online: http://www.nano.gov/NSINanomanufacturing (accessed on 27 November 2016).
- 97. Yayehrad AT, Siraj EA, Wondie GB, Alemie AA, Derseh MT, Ambaye AS. Could nanotechnology help to end the fight against COVID-19? Review of current findings, challenges and future perspectives. *Int J Nanomedicine* 2021;16:5713-43.
- Kandasamy G, Maity D. Multifunctional theranostic nanoparticles for biomedical cancer treatments — a comprehensive review. *Mater Sci Eng C Mater Biol Appl* 2021;127112199.
- Swisher JH, Jibril L, Petrosko SH, Mirkin CA. Nanoreactors for particle synthesis. Nat Rev Mater 2022;13:1-21.